



## Article

# Mineralogical and Geochemical Compositions of the Lopingian Coals and Carbonaceous Rocks in the Shugentian Coalfield, Yunnan, China: with Emphasis on Fe-Bearing Minerals in a Continental-Marine Transitional Environment

Xue Zheng <sup>1,2</sup> , Zhen Wang <sup>1,2</sup> , Lei Wang <sup>1,2</sup>, Yaguang Xu <sup>1,2</sup> and Jingjing Liu <sup>1,2,3,\*</sup>

<sup>1</sup> State Key Laboratory of Coal Resources and Safe Mining, China University of Mining and Technology, China; zhengxue1028@126.com (X.Z.); taylorsw110\_365@163.com (Z.W.); 13051873511@163.com (L.W.); 18230108848@163.com (Y.X.)

<sup>2</sup> College of Geoscience and Survey Engineering, China University of Mining and Technology (Beijing), Beijing 100083, China

<sup>3</sup> Shandong Provincial Key Laboratory of Depositional Mineralization & Sedimentary Mineral, Shandong University of Science and Technology, Qingdao 266590, China

\* Correspondence: liujingjing\_cumtb@outlook.com

Received: 28 July 2017; Accepted: 9 September 2017; Published: 14 September 2017

**Abstract:** This paper presents the mineralogical and geochemical compositions of coal benches and non-coal (carbonaceous rock benches, parting, roof and floor) samples from the No. 1 Coal in the Longtan Formation of the Permian-Lopingian epoch from the Shugentian Coalfield, eastern Yunnan Province, southwestern China. The coal is rich in Nb, Ta, Zr, and Hf, which were derived from the Kangdian Upland with the dominant compositions of the Emeishan basalt. The minerals identified in the samples include mixed-layer illite-smectite, kaolinite, quartz, siderite, and minor calcite, pyrite, anatase and ankerite. Albite and chamosite occur in the roof and floor samples. The parting sample (SGT1-2p) is characterized by abundant siderite (64.9%) and calcite (20.1%), and one carbonaceous rock sample SGT1-11 contained a large amount of pyrite (26.1%). Four factors were responsible for the geochemical and mineralogical compositions in the samples; namely, the terrigenous detrital materials transported from the Kangdian Upland, direct volcanic ash inputs, multi-stage inputs of hydrothermal fluids, and marine influences. The co-existence of siderite and pyrite was attributed to a continental-marine transitional environment.

**Keywords:** minerals in coal; trace elements in coal; Lopingian age; Yunnan Province

## 1. Introduction

The mineralogical and geochemical compositions of coal seams are influenced by many factors and geological processes that may have taken place over several periods [1–7]. Ren et al. [8] proposed five genetic types of enrichment for trace elements in Chinese coals, including source rock controlled, sedimentation-organism controlled, magma hydrothermalism controlled, deep and large fault-hydrothermalism controlled, and groundwater controlled types. Later, Ren et al. [9] and Dai et al. [10] suggested that volcanic activity and submarine exhalation are also factors affecting coal geochemistry and mineralogy. Subsequently, Dai et al. [11] reviewed the geochemistry of Chinese coals and proposed five types of genetic controls: source rock, marine environment, volcanic ash, hydrothermal fluids (including magmatic hydrothermal fluid, low temperature hydrothermal fluid, and submarine exhalation), and groundwater.

A number of studies have investigated the mineralogical and geochemical compositions of Lopingian coals and coal-bearing strata in southwestern China [12–20], which are dominantly controlled by Emeishan Large Igneous Province (ELIP) [21], as well as associated intense and frequent active volcanism [22–25] and related hydrothermal processes [10,26–32]. A number of the Lopingian coals in southwestern China are consequently rich not only in toxic elements [33,34], but also in critical metals that have potentially great economic significance [35–40]. ELIP was resulted from mantle plume activity between Guadalupian and Lopingian [41–45]. It is considered to be a potential cause of global climate change and bio-extinction events (end-Guadalupian mass extinction) [37,46]. After the uplift of the Emeishan mantle plume, a large-scale basalt erupted and overflowed, and ultimately formed the Kangdian Upland in the middle of ELIP [42], which is the dominant sediment-source region for the Lopingian coal-bearing strata in eastern Yunnan, western Guizhou, and southern Sichuan provinces (Figure 1) [21,23,47–49].

The Shugentian Coalfield is the one of the major coal producers in eastern Yunnan Province and No. 1 Coal is the major minable coal seam in the coalfield, although its thickness is generally 0.3 m, as revealed by the 201 drill-hoe. The strata overlying and underlying the No. 1 Coal contains high organic matter, and thus they are mined together with the coal as feed coals for local power plants, although the ash yield in these strata are over than 50% (from 54% to 72% and 64.5% on average) and are not generally considered to be coal. These strata are named as carbonaceous rock in this study. The elemental and mineralogical compositions in these strata, and their comparison with those in the coal, have not been addressed in detail in the Shugentian Coalfield.

This paper presents new data and discusses the mineralogical and geochemical compositions in No. 1 Coal, and in its underlying and overlying strata (carbonaceous rocks) in the Shugentian Coalfield. Particularly, we emphasized the formation of pyrite and siderite that co-exists in the samples, as well as factors responsible for mineralogical and elemental compositions.

## 2. Geological Setting

The Shugentian Coalfield is located in the Luoping County of eastern Yunnan Province, southwestern China (Figure 1). The sedimentary sequences in the Shugentian Coalfield include Devonian, Carboniferous, Permian, Triassic, Paleogene, Neogene, and Quaternary. The Carboniferous, Permian, and Triassic strata are widely distributed in the coalfield. No. 201 drill hole covers the Lopingian Longtan and Changxing formations, the Lower Triassic Kayitou and Feixianguan formations, and the Quaternary as well.

The coal-bearing sequences in the Shugentian Coalfield are the Lopingian Longtan Formation and the overlying Changxing Formation, containing seven to 12 coal seams (include four minable seams). The Longtan Formation, with a thickness of 124 to 209 m (average 166 m), is distributed in the western coalfield and is mainly composed of sandstone and mudstone, interbedded with thin layers of limestone (in 201 drill-hole, limestone is in the bottom of Longtan Formation, with a depth of ~650 m) and coal seams [23]. This formation was deposited in a continental-marine transitional environment [23] (Figure 1).

No. 1 Coal, the major minable coal seam in the coalfield, is located in the uppermost portion of the Longtan Formation (Figure 2) and has a thickness ranging from 0.47 to 3.94 m (2.02 m on average). The carbonaceous rock (ash yields vary from 50% to 72%, on air-dry basis), with macroscopic characteristics similar to coal, is calculated in the coal thickness. The roof strata of No. 1 Coal is sideritized siltstone and muddy siltstone, and the floor strata is dominated by mudstone.

The source region of the sediments in the Shugentian Coalfield is the Kangdian Upland, which is located to the west of the coalfield, and is major part of the Emeishan Large Igneous Province (ELIP) [21]. The ELIP is the only Large Igneous Province discovered in China, and has been widely investigated [44,50–54]. Also, the topography of the area to the east of the ELIP (high in west and low in east) that resulted from the ELIP, provided favorable sites for the peat development of eastern Yunnan, western Guizhou, and southern Sichuan Provinces [21].

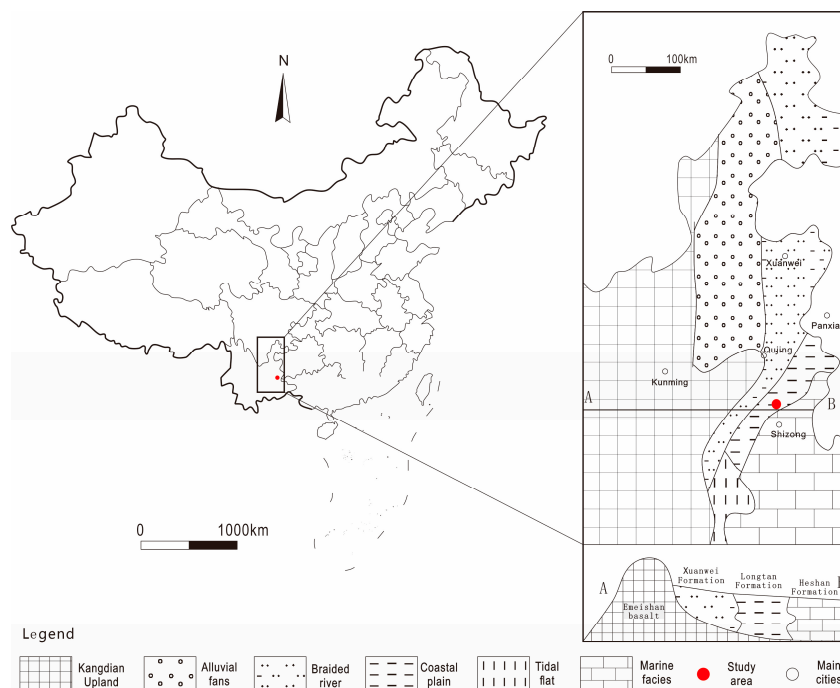


**Figure 1.** Location and sedimentary environments of the Lopingian Longtan Formation in the Shugentian Coalfield (modified from China Coal Geology Bureau, [23]).

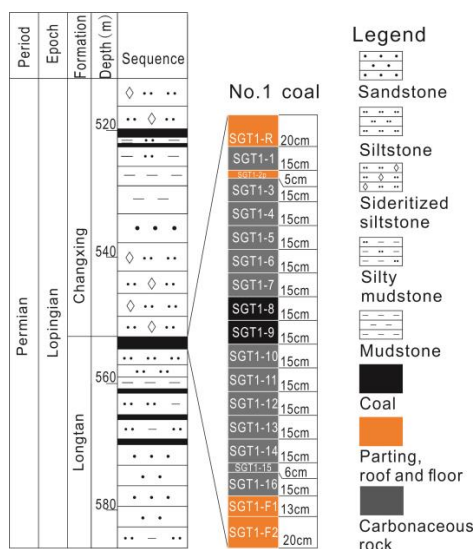


**Figure 2.** Sedimentary sequences of the 201 drill-hole in Shugentian Coalfield.

### 3. Samples and Analytical Methods

A total of 18 drill core bench samples including coal, carbonaceous rock, and host rocks (roof and floor) were collected from the No. 1 Coal in the 201 drill-hole in the Shugentian Coalfield. The samples were at a depth ranging from 552.75 to 555.49 m. The roof and floor samples were numbered as SGT1-R and SGT1-F1, SGT1-F2 respectively, while other coal and carbonaceous rock samples were named SGT1-1 to SGT1-16 from top to bottom (Figure 2). Sample SGT1-16 was not able to be collected in the present study because it has all been used for gas testing. The thickness of the collected floor sample is 20 cm, and that of the two roof samples, SGT1-F1 and SGT1-F2, are 13 and 20 cm, respectively.

The thicknesses of samples SGT1-2p and SGT1-15 are 5 cm and 6 cm, respectively; the thicknesses of other bench samples are all 15 cm.

All the samples were crushed and ground to pass 200-mesh for geochemical analysis. Proximate analysis was conducted following ASTM (American Society for Testing and Materials) Standards D3173-11 [55], D3175-11 [56], and D3174-11 [57]. The total sulfur and forms of sulfur in each coal were analyzed according to ASTM Standards D3177-02 [58] and ASTM Standard D2492-02 [59], respectively. Percentages of C, H, and N in coal benches were determined by an elemental analyzer (Vario MACRO, Elementar, Langenselbold, Germany). Mean random reflectance of vitrinite (percent Ro) in coal was determined according to ASTM Standard D2798-11a [60], using a Leica DM4500P microscope (at a magnification of 500×) equipped with a Craic QDI 302™ spectrophotometer (Leica Inc., Wetzlar, Germany).

The mineral composition was determined by X-ray powder diffraction (XRD). Low-temperature ashing of the coal benches was performed using an EMITECH K1050X plasma asher (Quorum Inc., Lewes, UK), prior to XRD analysis. XRD analysis of the low-temperature ashes (LTAs), as well as the non-coal samples, was performed on a powder diffractometer (D/max-2500/PC XRD, 40 kV, 100 mA) with Ni-filtered Cu-K $\alpha$  radiation and a scintillation detector (Rigaku, Tokyo, Japan). X-ray diffractograms of the LTAs and non-coal samples were subjected to quantitative mineralogical analysis using the Siroquant™ software system.

Modes of occurrence and some selected elements in some minerals in samples are determined by a field emission scanning electron microscope (SEM), equipped with an energy dispersive spectroscopy (EDS) (FE SEM-EDS). Samples were carbon-coated using a Quorum Q150T ES sputtering coater (Quorum Inc., Lewes, UK), or were not coated for low-vacuum SEM working conditions (60 bar), and were then mounted on standard aluminum SEM stubs using sticky conductive carbon tabs. The working distance of the FE SEM-EDS was 10 mm, beam voltage 20.0 kV, aperture 6, and spot size 5. The images were captured via a retractable solid state back-scattered electron detector.

The oxides of major elements, including SiO<sub>2</sub>, TiO<sub>2</sub>, Al<sub>2</sub>O<sub>3</sub>, Fe<sub>2</sub>O<sub>3</sub>, MgO, CaO, MnO, Na<sub>2</sub>O, K<sub>2</sub>O, and P<sub>2</sub>O<sub>5</sub>, were determined by X-ray fluorescence spectrometry (XRF; ARL ADVANT'XP+). Prior to XRF analysis, samples were ashed at a temperature of 815 °C, and the loss on ignition (LOI) was also determined at this temperature.

The concentrations of trace elements, except for Hg and F, were determined by inductively coupled plasma mass spectrometry (ICP-MS, Thermo Fisher (Waltham, MA, USA), X series II). The preparation of samples for ICP-MS was as follows: ~Fifty mg of the powdered samples (without ashing) of all coal and non-coal samples were digested using an UltraClave Microwave High Pressure Reactor (Milestone, Sorisole, BG, Italy). The digestion reagents were 5 mL 65% HNO<sub>3</sub>, and 2 mL 40% HF for coal samples and 2 mL 65% HNO<sub>3</sub> and 5 mL 40% HF for carbonaceous rock and host rock samples. The HNO<sub>3</sub> and HF for sample digestion were further purified through sub-boiling distillation before use. Inorganic Ventures standard references (CCS-1, CCS-4, CCS-5, and CCS-6) were used for calibration of trace element concentrations. In order to avoid interference by polyatomic ions, the collision/reaction cell technology of ICP-MS was performed to determine concentrations of As and Se in the samples, as outlined by Li et al. [61].

The concentration of Hg was determined on ~100 mg fresh samples (not ashed) in a Milestone DMA-80 analyzer (Milestone, Sorisole, BG, Italy), with a detection limit of 0.005 ng, and the linearity of the calibration was in the range 0–1000 ng. The concentration of fluorine was determined on ~500 mg raw samples (not ashed) by pyrohydrolysis using an ion selective electrode according to the method of ASTM D5987-96 [62].

## 4. Results

### 4.1. Proximate and Ultimate Analyses and Coal Rank

The proximate and ultimate analyses of coal and carbonaceous rock benches from No. 1 Coal are listed in Table 1. The ash yield in air dry basis was 34.1% on average, indicating media-high ash coal according to Chinese standard GB/T 15224.1-2010 [63]. The total sulfur content of the coal benches

was below 1%, and thus the coal could be classified as a low-sulfur coal [64]. The carbonaceous rock benches had ash yields ranging from 54.9% to 72.0% (64.5% on average, on air dry basis), volatile matter from 30.3% to 67.50% (44.4% on average, on air dry basis), and total sulfur content from 0.42% to 12.12% (2.83% on average).

The vitrinite reflectance values of two coal benches (1.8% for SGT1-8; 1.9% for SGT1-9), and the weighted average volatile matter (23.1%, dry and ash free basis) indicated a medium volatile bituminous coal according to the ASTM D 388-12 Standard [65].

**Table 1.** Proximate analysis (%), ultimate analysis (%), contents of total sulfur and forms of sulfur (%) of coal, carbonaceous rock, parting, roof and floor samples from 201 drillhole in Shugentian Coalfield.

Sample	Type	Thickness	M <sub>ad</sub>	A <sub>ad</sub>	V <sub>daf</sub>	C <sub>daf</sub>	H <sub>daf</sub>	N <sub>daf</sub>	S <sub>t,ad</sub>	S <sub>s,ad</sub>	S <sub>p,ad</sub>	S <sub>o,ad</sub>
SGT1-R	Roof	5cm	nd	78.10	nd	nd	nd	nd	0.04	nd	nd	nd
SGT1-1	C R	15 cm	0.54	60.99	nd	nd	nd	nd	0.83	nd	nd	nd
SGT1-2p	Parting	20 cm	nd	72.16	nd	nd	nd	nd	0.08	nd	nd	nd
SGT1-3	C R	15 cm	0.62	69.43	nd	nd	nd	nd	1.59	0.04	1.55	0.02
SGT1-4	C R	15 cm	0.78	68.41	nd	nd	nd	nd	1.24	0.02	1.42	bdl
SGT1-5	C R	15 cm	0.77	66.21	nd	nd	nd	nd	2.01	0.03	2.13	bdl
SGT1-6	C R	15 cm	0.70	71.99	nd	nd	nd	nd	2.52	0.02	2.36	0.15
SGT1-7	C R	15 cm	0.56	58.15	nd	nd	nd	nd	2.60	0.01	2.38	0.23
SGT1-8	Coal	15 cm	0.51	42.05	26.60	84.9	4.55	1.62	0.96	nd	nd	nd
SGT1-9	Coal	15 cm	0.57	25.77	19.69	89.1	4.41	1.68	0.94	nd	nd	nd
SGT1-10	C R	15 cm	0.65	57.78	nd	nd	nd	nd	1.82	0.05	1.80	bdl
SGT1-11	C R	15 cm	0.74	66.71	nd	nd	nd	nd	12.03	0.08	5.25	6.79
SGT1-12	C R	15 cm	0.78	54.87	nd	nd	nd	nd	5.64	0.04	3.96	1.68
SGT1-13	C R	15 cm	0.53	66.19	nd	nd	nd	nd	1.02	0.04	0.92	0.07
SGT1-14	C R	15 cm	0.63	66.61	nd	nd	nd	nd	0.58	nd	nd	nd
SGT1-15	C R	6 cm	0.75	70.48	nd	nd	nd	nd	0.42	nd	nd	nd
SGT1-F1	Floor	13 cm	1.02	78.80	nd	nd	nd	nd	0.40	nd	nd	nd
SGT1-F2	Floor	20 cm	nd	82.90	nd	nd	nd	nd	0.11	nd	nd	nd
C R-wa			0.67	64.52					2.81			

C R, carbonaceous rock benches; M, moisture; A, ash yield; V, volatile matter; S<sub>t</sub>, total sulfur; S<sub>s</sub>, sulfate sulfur; S<sub>p</sub>, pyritic sulfur; S<sub>o</sub>, organic sulfur; ad, as-received basis; daf, dry and ash-free basis. C R-Wa, weighted average for carbonaceous rock, based on thickness of bench interval; nd, not dot detected; bdl, below detect limit.

## 4.2. Geochemistry

### 4.2.1. Major-Element Oxides

The percentage of major-element oxides in the coal and carbonaceous rock benches of No. 1 Coal are listed in Table 2. Compared to average values for Chinese coals [11], TiO<sub>2</sub> was significantly enriched (concentration coefficient CC = 10.2; CC was the ratio of percentage of major-element oxides in the samples investigated vs. averages for Chinese coals); MnO was enriched (CC = 7.54); SiO<sub>2</sub>, Al<sub>2</sub>O<sub>3</sub>, K<sub>2</sub>O and P<sub>2</sub>O<sub>5</sub> were slightly enriched (CC = 2.34–3.31); and others were in the normal range (CC = 1–1.97).

The parting sample SGT1-2p was extremely enriched in MnO, CaO, and Fe<sub>2</sub>O<sub>3</sub>, but was depleted in SiO<sub>2</sub>, Al<sub>2</sub>O<sub>3</sub>, TiO<sub>2</sub>, K<sub>2</sub>O, P<sub>2</sub>O<sub>5</sub>, and Na<sub>2</sub>O (Table 2). The roof and floor samples were significantly enriched in MnO, and to a lesser extent, Fe<sub>2</sub>O<sub>3</sub>, and had higher content of CaO and MgO than coal and carbonaceous rock benches.

### 4.2.2. Trace Elements

The concentrations of trace elements in the coal benches and the averages for the world hard coals [66] are listed in Table 3. Compared with the averages for world hard coals, tantalum in the coal benches in this study is significantly enriched (CC = 10.2), while other lithophile elements including V, Zr, Nb, and Hf are enriched (CC = 5.2–7.4). Lithium, Sc, Cr, Co, Cu, Zn, Ga, and Th are also slightly enriched in the studied samples. Arsenic, Rb, Tl, and Bi are depleted (CC < 0.5), and the concentrations of the rest of the elements are close to those of the global average values for the world hard coals (Figure 3A).

The concentrations of trace elements in the carbonaceous rock benches are listed in Table 3. Compared to world clay and shale values [67], selenium is significantly enriched; elements V, Cu, Zr, Nb, Ta, and Hg were slightly enriched; B, Rb, Cs, Bi were depleted; other elements were close to the average of world clay and shale values in abundance (Figure 3B). Compared with the averages for world hard coals [66], tantalum, Nb and Zr in the carbonaceous rock benches in this study were significantly enriched ( $CC > 10$ ); Sc, V, Co, Cu, Zn, La and Hf were enriched ( $5 < CC \leq 10$ ); Be, B, Ge, As, Cs, Pb and U were in a normal range; Tl and Bi were depleted; other trace elements were slightly enriched (Figure 3C).

**Table 2.** Major-element oxides (%) in the Shugentian coal, carbonaceous rock, roof and floor strata.

Sample	Type	LOI/%	SiO <sub>2</sub>	TiO <sub>2</sub>	Al <sub>2</sub> O <sub>3</sub>	Fe <sub>2</sub> O <sub>3</sub>	MnO	MgO	CaO	Na <sub>2</sub> O	K <sub>2</sub> O	P <sub>2</sub> O <sub>5</sub>
SGT1-R	Roof	21.90	26.73	2.46	12.96	20.87	0.33	1.39	8.25	0.30	0.49	0.29
SGT1-1	C R	39.01	30.12	3.67	17.50	6.70	0.13	0.38	0.85	0.14	0.42	0.23
SGT1-2p	Parting	27.84	10.18	0.53	2.99	37.61	0.65	1.21	13.6	0.06	0.07	0.14
SGT1-3	C R	30.57	33.53	4.78	20.88	6.76	0.09	0.42	0.90	0.19	0.63	0.26
SGT1-4	C R	31.59	32.87	3.87	17.88	9.62	0.14	0.67	0.98	0.20	0.57	0.27
SGT1-5	C R	33.79	32.36	4.12	18.58	7.35	0.09	0.42	1.17	0.18	0.59	0.26
SGT1-6	C R	28.01	35.29	4.57	20.22	8.62	0.11	0.49	0.81	0.19	0.62	0.31
SGT1-7	C R	41.85	27.97	3.19	15.36	8.01	0.11	0.45	1.15	0.17	0.45	0.22
SGT1-8	Coal	57.95	20.04	2.26	11.95	5.05	0.08	0.33	0.95	0.11	0.28	0.15
SGT1-9	Coal	74.23	12.93	1.23	7.86	2.60	0.03	0.17	0.35	0.07	0.15	0.11
SGT1-10	C R	42.22	26.92	3.07	14.88	7.05	0.10	0.40	2.28	0.18	0.50	0.21
SGT1-11	C R	33.29	27.40	2.51	14.69	16.69	0.12	0.44	1.81	0.18	0.40	0.17
SGT1-12	C R	45.13	25.46	2.86	14.67	8.78	0.05	0.31	0.97	0.16	0.42	0.16
SGT1-13	C R	33.81	29.00	3.36	16.31	9.74	0.19	0.54	3.22	0.17	0.40	0.23
SGT1-14	C R	33.39	30.19	4.06	19.17	9.29	0.18	0.51	1.16	0.16	0.39	0.23
SGT1-15	C R	29.52	29.07	3.86	18.81	13.40	0.26	0.73	1.68	0.14	0.36	0.29
SGT1-F1	Floor	21.20	30.92	2.79	14.32	16.67	0.25	1.59	7.07	0.36	0.77	0.27
SGT1-F2	Floor	17.10	25.62	2.01	9.81	18.35	0.48	2.41	19.3	0.24	0.31	0.48
C-Wa			30.07	3.65	17.34	9.12	0.12	0.47	1.40	0.17	0.48	0.23
Chinese			8.47	0.33	5.98	4.85	0.015	0.22	1.23	0.16	0.19	0.09

The rows with gray shading are of carbonaceous rock (C R) benches. LOI, loss on ignition; C-Wa, weighted average for coal and carbonaceous rock, based on thickness of bench interval; Chinese coals, data from Dai et al. [11].

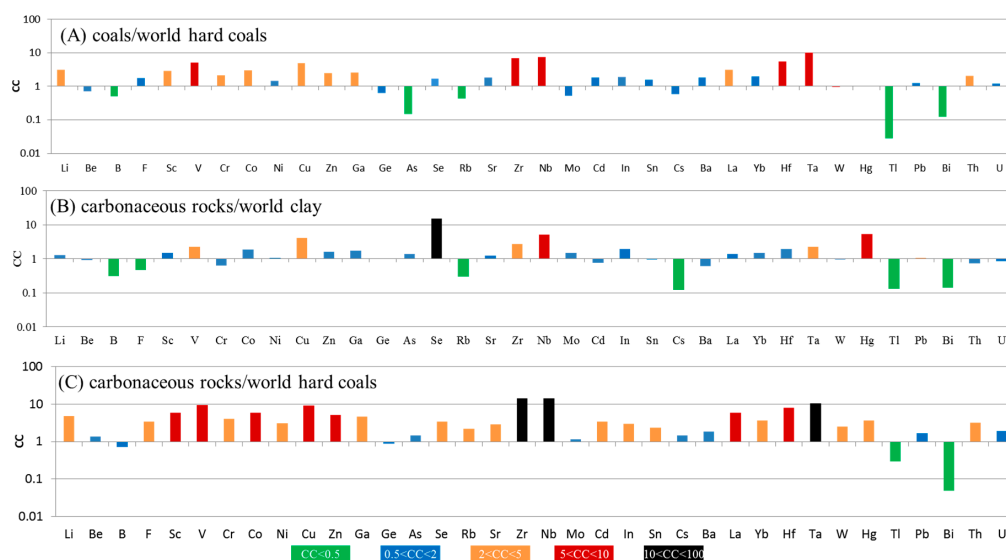


**Figure 3.** Concentration coefficient (CC) of trace elements in average Shugentian coal (A) and carbonaceous rock benches (B,C), Normalized by trace element concentrations in the world hard coals [66] and world clay [67].

**Table 3.** Trace elements (ppm) in the Shugentian coal, carbonaceous rock, roof and floor strata.

Sample	Li	Be	B	F	Sc	V	Cr	Co	Ni	Cu	Zn	Ga	Ge	As	Se	Rb	Sr	Zr	Nb
SGT1-R	34	2.17	27	231	32	241	60	32	47	123	108	18	1.6	2.0	1.7	14	525	317	40
SGT1-1	74	2.45	35	283	22	258	69	33	41	145	139	27	2.1	3.5	3.9	16	274	496	56
SGT1-2p	12	1.42	13	118	7.1	60	15	7.1	11	25	88	4.0	0.94	1.3	0.65	3.0	501	94	9.3
SGT1-3	88	3.16	38	318	29	386	92	52	67	195	176	35	2.5	7.9	3.9	24	328	661	75
SGT1-4	74	2.88	45	341	26	299	76	41	55	182	163	29	2.2	5.2	3.9	22	284	545	62
SGT1-5	78	2.82	38	299	26	322	86	46	62	173	165	32	2.2	6.7	5.4	23	348	560	65
SGT1-6	90	3.26	50	283	28	396	89	47	63	199	184	34	2.4	9.1	4.1	24	317	644	73
SGT1-7	66	2.46	27	284	21	248	65	32	49	148	133	25	2.0	5.7	4.9	16	284	460	51
SGT1-8	51	1.75	26	170	14	172	45	23	31	96	93	19	1.7	1.8	3.1	10	238	324	37
SGT1-9	35	1.13	20	119	7.9	119	28	13	18	60	48	13	1.3	0.87	2.3	5.2	125	184	22
SGT1-10	56	2.2	32	281	19	228	61	35	47	129	113	24	1.9	6.2	5.8	19	351	430	48
SGT1-11	13	4.13	25	205	4.8	2.5	5.2	1.8	63	12	92	22	1.5	71	14	263	40	437	32
SGT1-12	56	1.99	24	214	19	227	64	31	47	133	109	23	1.8	27	8.1	16	248	424	47
SGT1-13	67	2.34	26	267	22	248	68	32	44	139	139	24	2.1	3.9	3.3	15	416	463	52
SGT1-14	86	2.63	32	291	26	314	79	36	44	166	150	30	2.2	2.7	3.3	14	319	587	65
SGT1-15	85	2.69	36	359	25	310	80	34	41	166	161	29	2.1	2.9	2.9	17	373	574	65
SGT1-F1	34	2.53	27	350	20	247	101	39	58	136	120	23	1.9	4.9	2.6	28	691	390	45
SGT1-F2	28	1.78	15	564	29	188	146	37	74	76	107	22	1.7	2.0	0.75	16	748	275	12
C-wa	43	1.44	23	144	11	146	36	18	25	78	70	16	1.5	1.3	2.7	7.7	181	254	29
CR-wa	59	2.58	31	302	23	253	76	35	53	136	134	17	2.0	10	4.5	34	381	465	50
Coal	14	2	47	82	3.7	28	17	6	17	16	28	6	2.4	9	1.6	18	100	36	4
Clay	54	3	110	610	15	120	110	19	49	36	89	16	2	9.3	0.36	133	240	190	11
CC1	3.1	0.7	0.5	1.8	2.9	5.2	2.1	3.0	1.4	4.9	2.5	2.6	0.6	0.1	1.7	0.4	1.8	7	7.4
CC2	1.09	0.86	0.28	0.50	1.54	2.11	0.69	1.83	1.09	3.78	1.51	1.08	0.98	1.12	12.35	0.26	1.59	2.45	4.55
CC3	4.9	1.38	0.72	3.43	5.96	9.56	4.05	5.87	3.08	9.25	5.10	4.62	0.87	1.45	3.41	2.23	2.94	14.47	14.31

Table 3. Cont.

Sample	Mo	Cd	In	Sn	Sb	Cs	Ba	La	Yb	Hf	Ta	W	Hg	Tl	Pb	Bi	Th	U
SGT1-R	1.6	0.46	0.08	2.2	bdl	0.93	232	46	3.5	6.8	3.4	4.5	18	0.00	10	bdl	10	1.8
SGT1-1	1.7	0.65	0.12	3.2	bdl	1.3	211	59	3.8	9.2	3.6	2.3	98	0.02	9.3	0.08	10	4.2
SGT1-2p	0.29	0.18	0.02	0.52	bdl	0.31	136	11	1.4	2.1	1.9	2.4	15	bdl	3.2	bdl	1.2	0.61
SGT1-3	3.1	0.89	0.15	4.3	bdl	1.8	374	81	4.7	13	4.7	2.8	175	0.06	12	0.06	12	4.9
SGT1-4	2.0	0.66	0.13	3.4	bdl	1.6	259	65	4.0	9.6	3.3	1.9	114	0.02	9.4	0.08	10	4.1
SGT1-5	2.7	0.75	0.14	3.8	bdl	1.7	267	68	3.9	11	3.6	3.0	178	0.05	16	0.05	10	4.1
SGT1-6	2.8	0.80	0.15	4.1	bdl	1.8	259	75	4.1	13	4.5	2.4	231	0.12	13	0.05	11	4.5
SGT1-7	2.5	0.59	0.11	2.9	bdl	1.3	246	55	3.3	8.3	2.7	3.5	216	0.13	15	0.08	8.5	3.3
SGT1-8	1.6	0.43	0.09	2.5	bdl	0.80	338	41	2.4	8.2	4.3	1.5	106	0.03	12	0.14	6.5	2.5
SGT1-9	0.60	0.30	0.06	2.0	bdl	0.47	201	28	1.6	4.9	1.8	0.34	94	0.01	10	0.13	6.6	2.1
SGT1-10	1.9	0.60	0.11	2.8	bdl	1.4	355	52	3.0	7.8	2.4	2.2	167	0.08	17	0.08	7.7	3.0
SGT1-11	2.1	0.56	0.07	3.0	bdl	3.3	508	84	4.2	9.7	0.9	0.02	1987	0.92	36	bdl	21	4.0
SGT1-12	4.4	0.64	0.10	2.7	bdl	1.3	247	50	2.9	7.3	2.4	3.0	801	0.48	22	0.07	6.6	2.7
SGT1-13	1.7	0.61	0.11	2.9	bdl	1.2	208	57	3.3	8.2	2.9	4.4	118	0.08	11	0.04	7.1	2.7
SGT1-14	1.7	0.73	0.13	3.6	bdl	1.2	199	70	3.8	11	3.7	1.7	81	0.01	8.6	0.04	8.7	3.4
SGT1-15	1.5	0.76	0.13	3.4	bdl	1.3	208	69	3.8	9.8	3.3	2.6	74	0.03	10	0.03	8.7	3.3
SGT1-F1	1.3	0.58	0.10	2.4	bdl	1.4	248	49	2.8	6.6	2.3	2.9	56	0.06	18	bdl	5.0	1.4
SGT1-F2	0.39	0.44	0.06	bdl	bdl	0.63	122	60	3.0	5.2	bdl	0.54	17	bdl	6.9	bdl	7.1	0.83
C-wa	1.1	0.36	0.07	2.2	bdl	0.64	270	34	2.0	6.5	3.1	0.94	100	0.02	11	0.13	6.6	2.3
C R-wa	2.0	0.62	0.11	2.8	bdl	1.4	259	65	3.7	8.8	2.8	2.5	281	0.13	14	0.03	9.4	3.1
Coal	2.1	0.2	0.04	1.4	1	1.1	150	11	1	1.2	0.3	0.99	100	0.58	9	1.1	3.2	1.9
Clay	1.6	0.91	0.06	3.5	1.3	13	460	48	2.5	5	1.4	2.6	68	1.3	14	0.38	14	4.3
CC1	0.5	1.8	1.9	1.6	bdl	0.6	1.8	3.1	2.0	5.4	10.2	0.9	1.0	0.0	1.2	0.1	2.1	1.2
CC2	1.27	0.69	1.73	0.81	bdl	0.11	0.56	1.36	1.49	1.75	2.01	0.97	4.14	0.10	0.99	0.08	0.67	0.72
CC3	1.14	3.41	3.05	2.38	bdl	1.46	1.88	5.94	3.73	8.15	10.48	2.50	3.68	0.30	1.68	0.05	3.18	1.95

C-wa: weighted average for coal, based on thickness of coal bench interval; Coal: the world hard coals, data from Ketris and Youdovich [66]. CC1: C-wa/Coal. C R-wa, weighted average for carbonaceous rock(C R) benches, based on thickness of coal bench interval; clay, the world clay, data from Grigoriev [67]. CC2: C R-wa/Clay; CC3: C R-wa/Coal.

### 4.2.3. Rare Earth Elements and Yttrium

Based on the classifications by Seredin and Dai [68], the rare earth elements and Yttrium (REY, or REE if Y is not included) are divided into three groups: light rare earth elements and yttrium (LREY: La, Ce, Pr, Nd, and Sm), medium REY (MREY: Eu, Gd, Tb, Dy, and Y), and heavy REY (HREY: Ho, Er, Tm, Yb, and Lu). Compared to the upper continental crust [69], three REY enrichment types were identified: L-type ( $La_N/Lu_N > 1$ ), M-type ( $La_N/Sm_N < 1$ ,  $Gd_N/Lu_N > 1$ ), and H-type ( $La_N/Lu_N < 1$ ) Seredin and Dai [68].

The average concentration of REY in coal benches was 199  $\mu\text{g/g}$ , higher than the global average values of hard coals (68.6  $\mu\text{g/g}$ , [66]). The average concentration of REY in the carbonaceous rock benches was 391  $\mu\text{g/g}$ , higher than that of the global average value for clay and shale values (226  $\mu\text{g/g}$ , [67]). The REY in coal benches had L- ( $La_N/Lu_N > 1$ ) and M-type enrichment ( $La_N/Sm_N < 1$ ,  $Gd_N/Lu_N > 1$ ) and were characterized by positive Eu anomalies (Figure 4B). Samples SGT1-R and SGT1-2p were characterized by H- ( $La_N/Lu_N < 1$ ) and M-types ( $La_N/Sm_N < 1$ ,  $Gd_N/Lu_N > 1$ ), and had distinct positive Eu anomalies (Figure 4A). Sample SGT1-11 was characterized by L-type ( $La_N/Lu_N > 1$ ) and a strongly negative Eu anomaly (Figure 4C). The Eu anomaly is calculated as [70]:

$$Eu_N/Eu_N^* = Eu_N / [(Sm_N \times 0.67) + (Tb_N \times 0.33)]$$

$Eu_N$  is the ratio of Eu concentration in the investigated samples vs. the Eu concentration in the UCC [70]. Floor and other carbonaceous rock benches are of L-type ( $La_N/Lu_N > 1$ ) and M-type ( $La_N/Sm_N < 1$ ,  $Gd_N/Lu_N > 1$ ), and are characterized by positive Eu anomalies (Figure 4A,C).

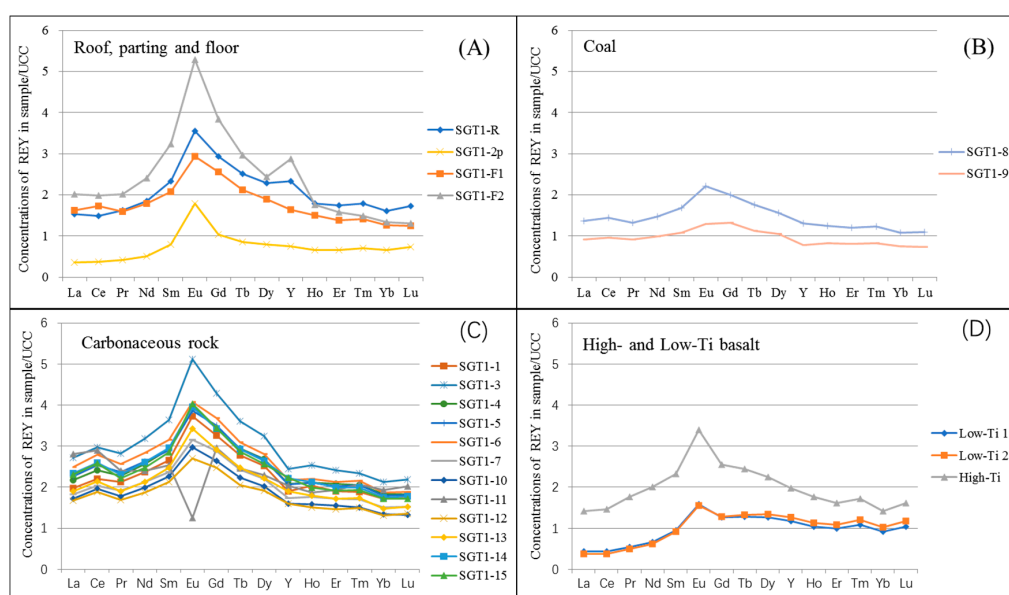


**Figure 4.** Distribution patterns of rare earth elements and yttrium (REY) of samples in Shugentian coalfield (A–C). REY are normalized by the Upper Continental Crust (UCC) [67]. Data for high- and low-Ti alkali basalts (D) are from Xiao et al. [71].

### 4.3. Mineralogy

#### 4.3.1. Mineral Composition

The minerals in the coal LTAs of SGT1-8 and SGT1-9 were composed of mixed-layer illite/smectite (I/S) (24.6% and 37%, respectively), kaolinite (35.8% and 16%, respectively), and quartz (15.9% and 26%, respectively). Other minerals were at a low percentage, e.g., siderite (9.1% and 9.7%, respectively), pyrite (4.8% and 5.3%), anatase (5.1% and 4.5%), calcite (3% and 0.5%), and ankerite (1.7% and 1%) (Table 4).



### 4.3.2. Comparison between the Mineralogical and Chemical Compositions

The comparison between the percentages of major element oxides ( $\text{SiO}_2$ ,  $\text{Fe}_2\text{O}_3$ ,  $\text{Al}_2\text{O}_3$ ,  $\text{CaO}$ ,  $\text{MgO}$ , and  $\text{TiO}_2$ ) calculated from the XRD-Siroquant, and XRF results are presented as X-Y plots (Figure 6), based on the methods based on Ward et al. [72] and Dai et al. [73,74]. Both coal benches and non-coal samples data sets were calculated on a  $\text{SO}_3$ -free basis. The points for  $\text{SiO}_2$ ,  $\text{Fe}_2\text{O}_3$ ,  $\text{Al}_2\text{O}_3$  and  $\text{CaO}$  in the plots were close to the equal lines. This indicates that XRD-Siroquant produced reliable results for the major minerals (kaolinite, quartz, siderite and calcite) in coal benches and non-coal samples. However, the majority of the points in the plots of  $\text{SiO}_2$  and  $\text{Fe}_2\text{O}_3$  fell slightly above the equality line, indicating an over-estimation of  $\text{SiO}_2$  and  $\text{Fe}_2\text{O}_3$  calculated from XRD-Siroquant relative to XRF results. The majority of the points for the plots of  $\text{Al}_2\text{O}_3$  and  $\text{CaO}$  fell slightly below the equality line, indicating an under-estimation of  $\text{Al}_2\text{O}_3$  and  $\text{CaO}$  as calculated from XRD-Siroquant, relative to XRF results. The SEM-EDS data, the Si/Al ratio of kaolinite in the No. 1 Coal of Longtan Formation coal benches and non-coal samples higher than the standard values (1.18) (Figure 7), agree with this; The siderite in the coal benches and non-coal samples of the present study contained some Ca (Figure 8); however, the present study calculated siderite as  $\text{FeCO}_3$ . Most of the points in the plot for  $\text{MgO}$  fell below the equality line, this was because Mg occurs in siderite as indicated by SEM-EDS data (Figure 8).

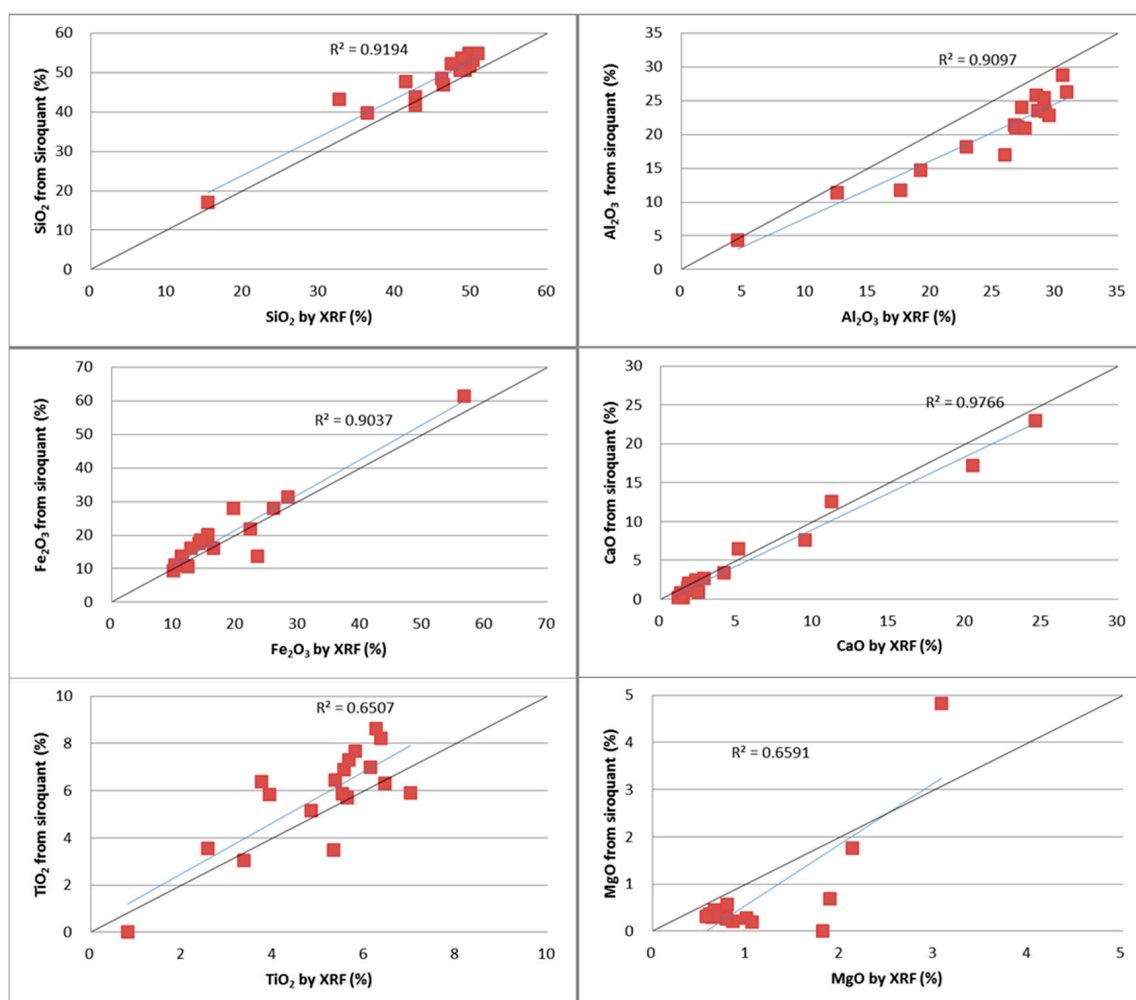


**Figure 6.** Comparison of observed normalized oxide percentages from chemical analysis ( $x$ -axis) to oxide percentages for sample ash inferred from XRD analysis data ( $y$ -axis). The diagonal line represents equality in each plot.

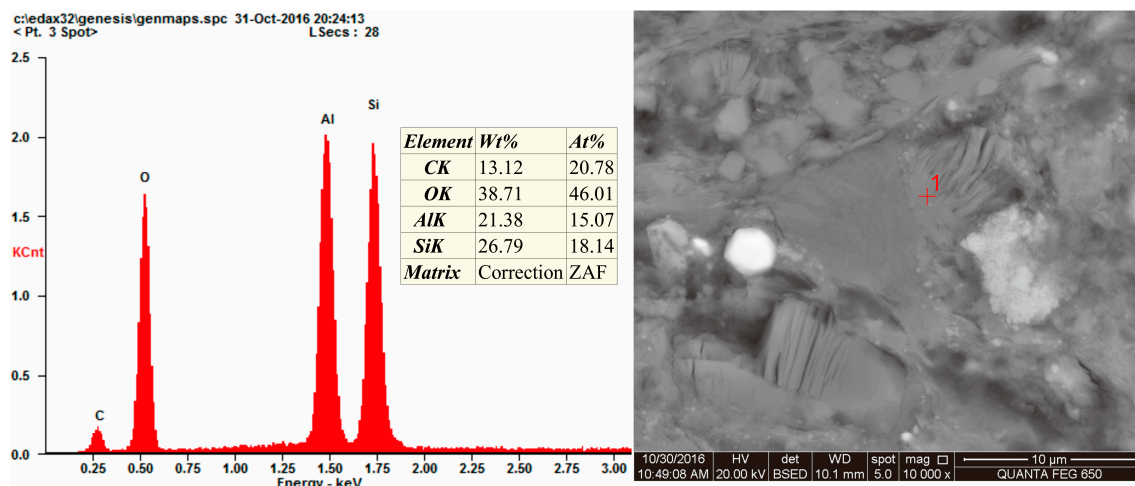


**Figure 7.** Scanning electron microscopy (SEM) backscattered electron image of minerals and EDS spectrum of spot 1 (SGT1-11).

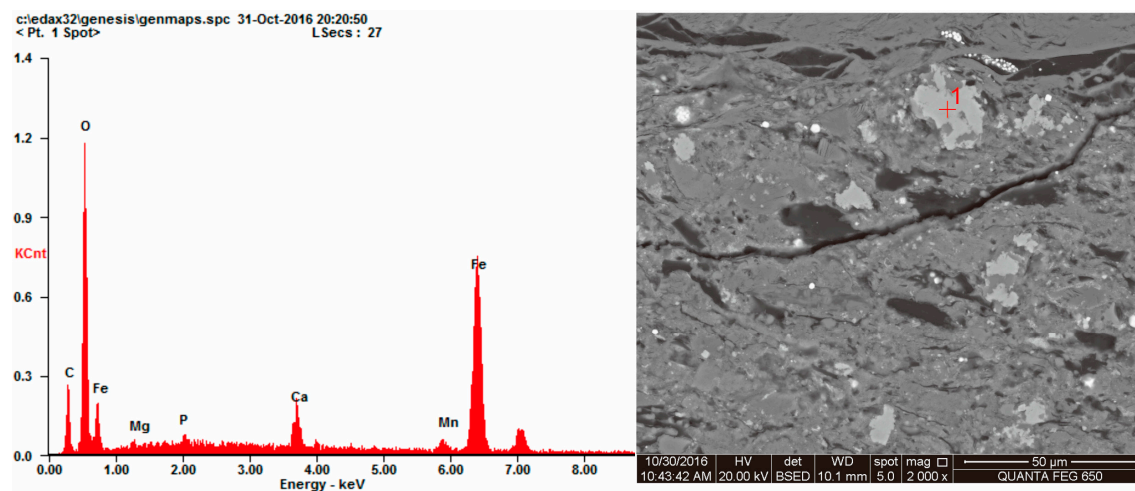


**Figure 8.** SEM backscattered electron image of minerals and EDS spectrum of spot 1 (SGT1-11).

#### 4.3.3. Modes of Occurrence of Minerals in Coal and Carbonaceous Rock Benches

The minerals in the coal LTAs of SGT1-8 and SGT1-9 were composed of mixed-layer illite/smectite (I/S) (24.6% and 37%, respectively), kaolinite (35.8% and 16%, respectively), and quartz (15.9% and 26%, respectively). Other minerals were present at a low percentage, e.g., siderite (9.1% and 9.7%, respectively), pyrite (4.8% and 5.3%), anatase (5.1% and 4.5%), calcite (3% and 0.5%), and ankerite (1.7% and 1%) (Table 4).

Carbonate minerals identified in almost all the samples investigated in this study (Table 4) included siderite, calcite, and ankerite. Siderite was present in all samples, with the highest content in SGT1-2p. Siderite mainly occurs as massive, syngenetic nodules, cell-infillings, and epigenetic cleat-infillings (Figure 9). The cleat-infilling siderite cuts across the cell-infilling kaolinite, indicating that the former formed later than the latter. Siderite contains traces of Ca, Mn, and Mg (Figure 8), which substitutes for Fe. Calcite mainly occurs as vein-fillings (Figure 9A,B and Figure 10A,C), and massive aggregates of crystals together with pyrite (Figure 11C). The euhedral calcite crystals show two groups of approximately orthogonal cleavages (Figure 10D). Ankerite was identified in several samples (SGT1-R, 1-8, 1-9, 1-11, 1-F1, 1-F2) under SEM-EDS and by XRD, and co-exists with siderite in the cavities of the organic matter (Figure 9E,F).

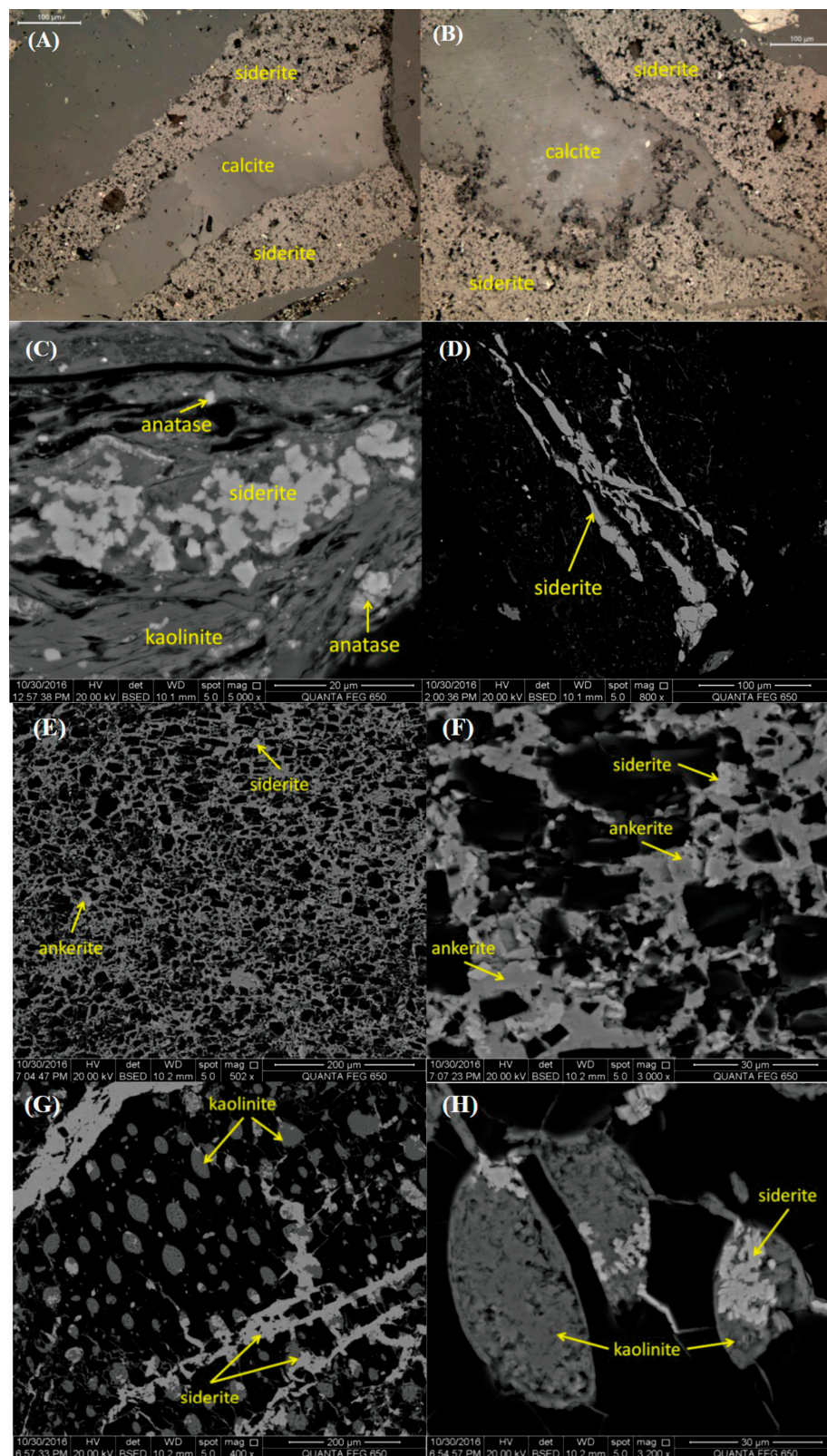


**Figure 9.** Carbonate minerals and kaolinite in samples investigated. (A,B) Massive siderite and vein like calcite, optical microscope, reflected light; (C) syngenetic nodules siderite in SGT1-9 sample; (D) rod-like siderite; (E,F) organic matter-bound siderite and ankerite; (G) vein infilling siderite and cell infilling kaolinite; (H) Cell infilling siderite and kaolinite; (D–H) are SEM back-scattered images of SGT1-11 sample.

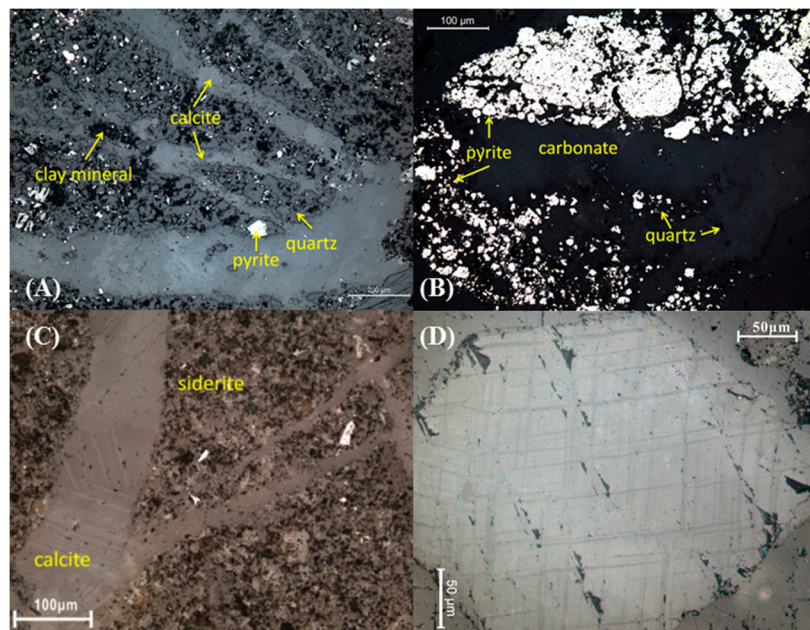


**Figure 10.** (A) Vein-like calcite; (B) massive carbonate mineral and pyrite; (C) vein like calcite and massive siderite; (D) euhedral calcite.

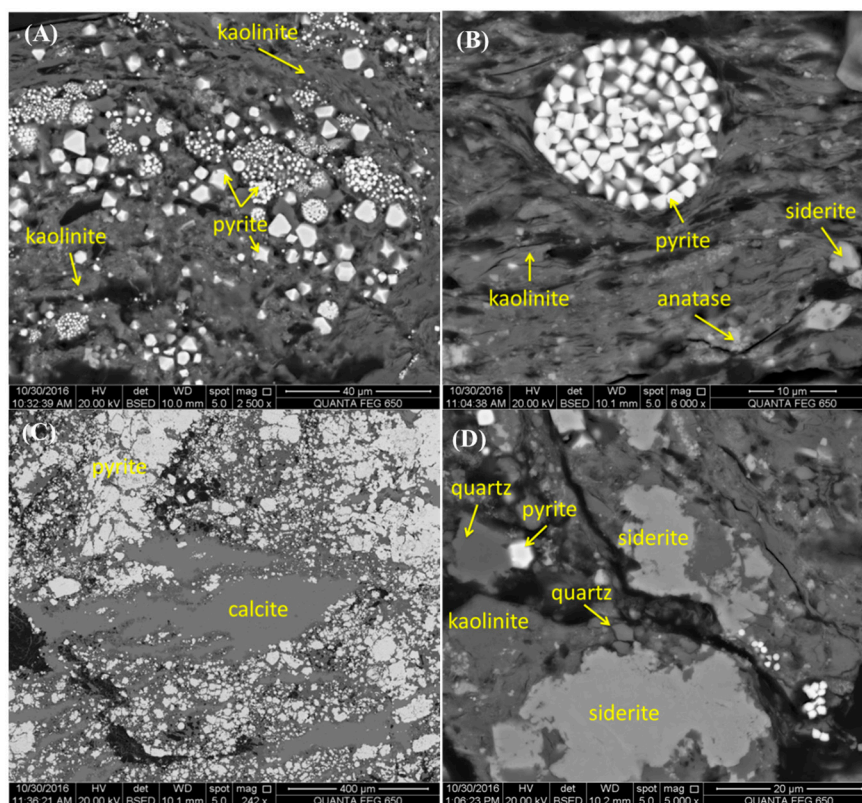


**Figure 11.** Pyrite in the SGT1-11 sample. (A) Framboidal and euhedral pyrite in kaolinite matrix; (B) framboid with euhedral pyrite crystals; (C) massive pyrite connected with calcite; (D) single euhedral pyrite. SEM back-scattering images.

The content of pyrite varied greatly in different bench samples of No. 1 Coal, and the highest pyrite content occurred in carbonaceous rock bench SGT1-11 (26.1%). It occurred as framboidal,

massive, and euhedral crystal forms (Figure 11). The spherical framboids were aggregates of euhedral discrete crystals, which were uniformly distributed within the framboids (Figure 11B).

The framboidal pyrite in the present study, which is associated with clay minerals and euhedral pyrite, was of inorganic origin, and had a similar formation mechanism with euhedral pyrite [75]. The framboidal pyrite was formed during peat development or in early diagenesis [31,64,75–77]. Rickard et al. [78] and Luther [79] suggested that the single crystal pyrite of framboids formed at low temperature (25 °C).

Quartz was identified in all coal and carbonaceous rock benches in the present study, and its amount seemed to be similar in all samples. Massive quartz and/or clay mineral distributes in organic matter (Figure 12A,B). To a lesser extent, quartz occurred as individual rounded grains, with the major axis being longer than 100 µm, surrounded by syngenetic clay minerals, indicating a detrital origin (Figure 12C,D).

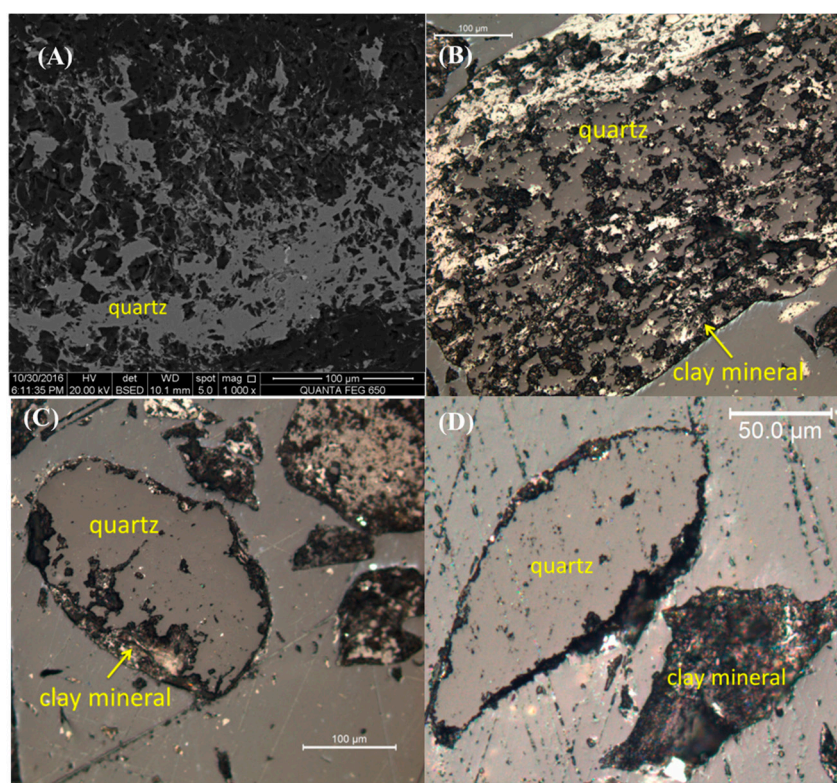


**Figure 12.** Quartz in the coal and non-coal samples. (A,B) Massive quartz in SGT1-9 and SGT1-3 samples; (C,D) detrital quartz coated by clay mineral in SGT1-3 and SGT1-1 samples; (A) is a SEM back-scattering image; (B–D) are under optical microscopy (reflected light).

Clay minerals in the present study included kaolinite, mixed-layer illite and smectite (I/S), and chamosite. Kaolinite was the most common clay mineral, and occurred as cell-infillings and fissure-infillings (Figure 13A,B), a book-like form, and as a matrix of other minerals (Figure 13C,D). Mixed-layer I/S clay was identified by XRD in most samples while chamosite was found only in the floor samples (SGT1-F1 and SGT1-F2) (Figure 5).

Anatase occurs as fine crystal grains and is scattered in the kaolinite matrix (Figures 9C, 11B and 13C). Apatite occurred as a detrital form and as fine grains, both of which were coated by kaolinite (Figure 14A,B). Detrital apatite was derived from terrestrial sources or volcanic ash [22,76,80–82]. Albite occurred as euhedral crystals, and was distributed in the matrix of siderite (Figure 14C). Florencite was found in the matrix of organic matter (Figure 14D).

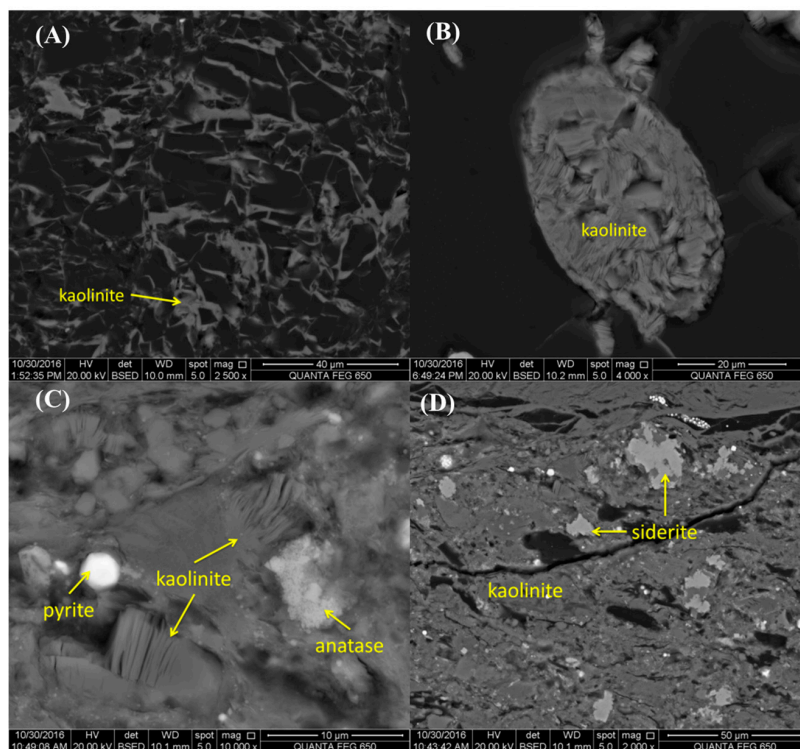


**Figure 13.** Kaolinite in Shugentian coal and non-coal samples, (A,B) Fissure-infilling and cell-infilling kaolinite in SGT1-9 sample; (C) book-like kaolinite in SGT1-11 sample; (D) kaolinite occurs as matrix of other minerals (siderite, pyrite and anatase) in SGT1-11 sample. SEM back-scattering images.

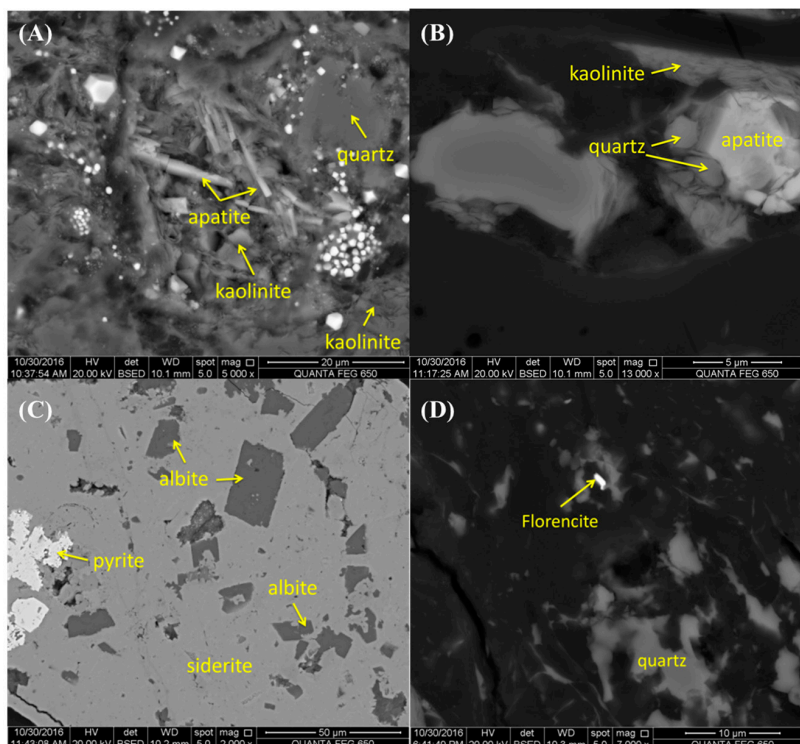


**Figure 14.** (A) Apatite, kaolinite, quartz and pyrite; (B) apatite coated by kaolinite; (C) albite in siderite matrix; (D) florencite (REE-bearing mineral) in organic matter matrix. SEM back-scattering images, (A–C) are from SGT1-11 sample; (D) is from SGT1-9 sample.

## 5. Discussion

### 5.1. Influencing Factors on Geological and Mineralogical Compositions

The geochemical and mineralogical characteristics of No. 1 Coal in the Longtan Formation indicated that they were probably influenced by four factors: input from the sediment-source region, sea water influence, volcanic ash input, and injection of hydrothermal fluids.

#### 5.1.1. Sediment-Source Region

As with other Lopingian coalfields in western Guizhou, eastern Yunnan, southern Sichuan, and Chongqing [11,21,23], the sediment-source region for the Shugentian Coalfield was the Kangdian Upland, based on the following evidence:

1. The elevated concentrations of Sc, V, Cr, Co, Ni and Zn in the No. 1 Coal and carbonaceous rocks (Figure 3A,B), which were derived from basalts in the Kangdian Upland.
2. The ratios of  $\text{Al}_2\text{O}_3/\text{TiO}_2$  of the coal and carbonaceous rock benches exclusively fall in the area between 3 to 8 (Figure 15), indicating that the terrigenous source of the studied samples is of mafic composition [83]. A number of studies showed that the ratio  $\text{Al}_2\text{O}_3/\text{TiO}_2$  is a reliable indicator for identifying the sediment-source regions not only for normal sediments but also for coal [32,80,83–87].
3. It has been reported that quartz derived from the Kangdian Upland is abundant in the Lopingian coals in southwestern China [16]. The high authigenic quartz identified in the coal and carbonaceous rock benches (Figure 12A,B) was probably deposited from silica-bearing solutions originating from the weathering of basaltic rocks in the Kangdian Upland [48].
4. All coal benches and non-coal samples (carbonaceous rock benches, parting, and roof and floor samples) have strong positive Eu anomalies (1.37 on average), except SGT1-11 (Figure 4). Eu anomalies require both high-temperature ( $>250^\circ\text{C}$ ) and extreme reducing conditions [70,88,89]. For coals, Eu anomalies inherited from rocks within the sediment source region or affected by high-temperature hydrothermal fluids [70]. In Shugentian Coalfield, with no evidence indicating high temperature hydrothermals, the positive Eu anomalies are derived from tholeiitic basalts of the Kangdian Upland. Furthermore, The REY distribution patterns of coal, carbonaceous rock (except SGT1-11), parting, and roof and floor in the Shugentian Coalfield, characterized by M-type enrichment and positive Eu anomalies (Figure 15), are similar to those for low-Ti and high-Ti basalts from the western Emeishan Large Igneous Province as reported by Xiao et al. [71].

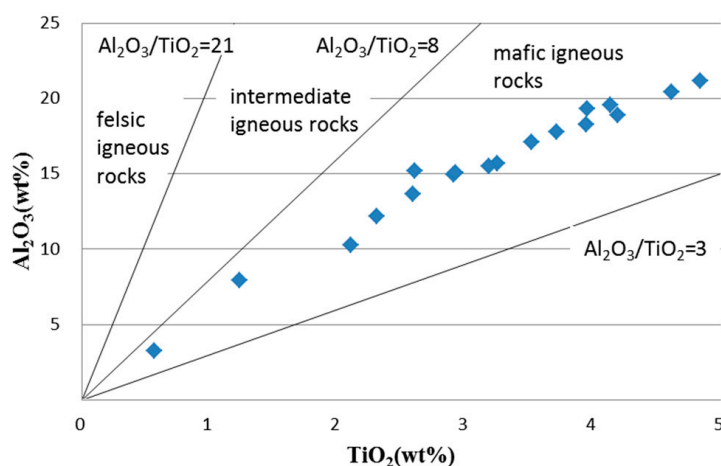


Figure 15. Bivariate plot for  $\text{Al}_2\text{O}_3$  and  $\text{TiO}_2$  in No. 1 coal seam of the Shugentian coalfield.

### 5.1.2. Volcanic Ash Input

Elemental and mineralogical compositions in carbonaceous rock bench SGT1-11 are distinctive in comparison with other coal and carbonaceous rock benches. The depleted concentrations of Sc, V, Cr, and Co in sample SGT1-11 (Table 3) indicate that sediments in this bench were not derived from the Kangdian Upland, which however is rich in these elements. The sample was characterized by a strong negative Eu anomaly ( $\delta\text{Eu} = 0.5$ ) (Figure 4D), quite different to those in other coal and carbonaceous rock benches. Although sediments derived from the Emeishan intermediate-felsic rocks, which are located on the top of the Emeishan mantle plume, have strong negative Eu anomalies [86], these sediments are always in the lowermost portions of the Longtan Formation [21,49,86]. The coal and carbonaceous rock horizons in this study, however, were in the uppermost portion of the Longtan Formation. Apatite, euhedral albite, and sharp-edged quartz (Figure 14A–C), kaolinite associated with quartz, and apatite and anatase (Figures 13C and 14A,B), can also be indicators for volcanic ash inputs into palaeomire and/or detrital inputs from the ELIP. [39,76,90–92].

### 5.1.3. Injection of Multi-Stage Hydrothermal Fluids

A number of studies showed that hydrothermal fluids have significantly influenced the geochemical and mineralogical composition of Lopingian coals in southwestern China (e.g., [26,48,86,93–95]). The evidence for the No. 1 Coal and carbonaceous rock benches subjected to hydrothermal fluids includes: (1) Chamosite identified in samples SGT1-F1 and SGT1-F2 by XRD. Previously studies [29,30,48] showed that the formation of chamosite in eastern Yunnan coals was related to hydrothermal fluids, either deposited from Fe-rich hydrothermal fluids [29] or formed via interaction between kaolinite and Fe-Mg-rich fluids during early diagenesis [30]; (2) Florencite identified in the samples (Figure 14C). This is a secondary REE-bearing mineral related to hydrothermal fluid [38,86,96]; (3) Fracture-filling siderite (Figure 9C,D) and fracture-filling calcite in the samples. These carbonate minerals indicate epigenetic solution precipitation; (4) Abundant siderite (65%) and calcite (20%) in sample SGT1-2p. Their occurrence may indicate Ca- and Fe-rich solutions injected into the coal. This horizon had a low REY value, while its underlying SGT1-3 had a higher REY concentration compared to its adjacent seams, indicating a hydrothermal leaching occurred to the parting, and the leached REY was ultimately deposited in the underlying horizons; (5) SGT1-11 showed a Gd-maximum, which may have resulted from the injections of acid solutions, including high  $\text{pCO}_2$ -water in coal basin [97].

### 5.1.4. Sea Water

Previous studies indicated that the Longtan Formation in eastern Yunnan and western Guizhou was deposited in a continental-marine transitional environment [4,15,20,85,86,98,99]. The high concentration of some elements (e.g., K, Mg, Li, F, Sr) in the samples, which were higher in seawater than in freshwater [100], may also indicate a marine influence. In addition, the high S and pyrite content of the carbonaceous rock (Table 1) also suggests an influence by seawater, sulfate-rich lake waters, or groundwater [63,101–103].

The high ratio of Sr/Ba in carbonaceous rocks also indicates the influence of seawater.  $\text{Sr/Ba} < 1$  usually represents continental sediments while  $\text{Sr/Ba} > 1$  usually suggest marine sediments [104]. Coal benches in No. 1 Coal in the coalfield had a ratio of  $\text{Sr/Ba} < 1$ , and most carbonaceous rock benches, however, had  $\text{Sr/Ba} > 1$ , indicating that coal benches of the coalfield were deposited during the regression stage. It should be noted that the roof, parting and floor samples (SGT1-R, SGT1-2p, SGT1-F1, SGT1-F2) contained abundant calcite, which in most cases is of epigenetic origin and may contain Sr as an isomorphism with Ca, and thus, the ratio of Sr/Ba could not be used as an indicator of marine influence.

Gadolinium in common Chinese coals generally shows very weak negative anomalies [70]. However, all the studied coal benches and non-coal samples had positive Gd anomalies (from 1.16 to 1.26, with an average of 1.19). In addition to low-Ti and high-Ti basalt of the Kangdian

Upland, which have an average Gd anomaly of 1.07 [71], seawater and/or hydrothermal fluids also be responsible for positive Gd anomalies [70]. It was reported that seawater generally shows positive Gd anomalies [105,106].

## 5.2. Major Fe-Bearing Minerals

The major Fe-bearing minerals in No. 1 Coal are pyrite and siderite, both of which coexist in all coal and carbonaceous rock benches (Table 4). Framboidal pyrite, which generally indicate a reducing condition and an authigenic origin [64,75,107–111], was identified in some samples investigated in this study (Figure 11A,B). The pyrite with irregular shape was scattered in the matrix of siderite (Figure 16). Syngenetic pyrite is generally indicative of deposition in marine influenced environment or sulfate-rich lake waters or groundwaters [63,101–103], and abundant siderite indicates non-marine, at least waters with a low sulfate content [103]. However, siderite has been observed in many cases to coexist with syngenetic pyrite [72,103,112]. When  $\text{SO}_4^{2-}$  is totally reduced to  $\text{S}^{2-}$ , and iron occurs in surplus, minor siderite will be formed in marine-influenced environments. In sulfate-containing freshwater, pyrite can form together with siderite in a reductive condition [113]. Pyrite and siderite could also form sequentially in freshwater environments due to the change of from neutral to acidic conditions. In neutral to slightly alkaline environments, siderite can form, whereas pyrite is typical for slightly acidic settings (which are optimal for the sulfate-reducing bacteria) [76,114].

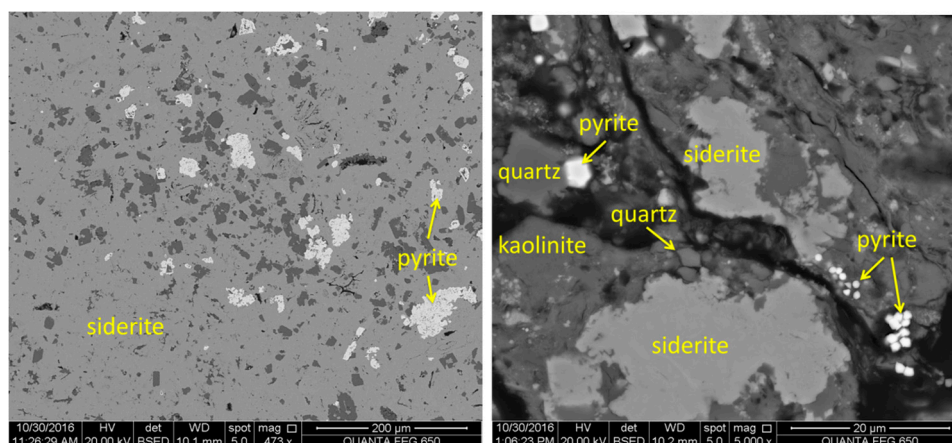


Figure 16. Pyrite and siderite coexisted in SGT1-11, SEM back-scattering images.

Contents of siderite and pyrite showed a negative correlation in No. 1 coal and carbonaceous rock. The abundant pyrite and less abundant siderite formed when sea water was injected into the coalfield, and vice versa.

## 6. Conclusions

Minerals in the Shugentian coal and carbonaceous rock samples consisted of carbonates (siderite and calcite), kaolinite, mixed layer I/S, quartz, pyrite, and minor amounts of anatase, ankerite, albite, and chamosite. The coal benches were significantly enriched in Nb, Ta, Zr, Hf, and V ( $\text{CC} > 5$ ), and slightly enriched in REY.

The sediment-source region (the Kangdian Upland), volcanic ash inputs, multi-stage hydrothermal fluid activities, and marine influence were responsible for the geochemical and mineralogical anomalies in the Shugentian coal and carbonaceous rock samples.

Minerals in sample SGT1-2p were dominated by carbonates (64.9% siderite and 15.9% calcite) that may have originated from hydrothermal fluid, which was enriched in iron and calcium. SGT1-11 had a high total sulfur content (12.03%) and a high organic sulfur content (6.79%), as well as a strong negative  $\delta\text{Eu}$  value (0.46), probably due to the input of felsic volcanic ash to peat swamp during peat accumulation.

The common occurrence of both siderite and pyrite in the same sample is attributed to the continental-marine transitional environment. Furthermore, sufficient iron in a marine environment and changing acidity in a freshwater environment are also essential.

**Acknowledgments:** This research was supported by the National Natural Science Foundation of China (No. 41420104001), the National Key Basic Research Program of China (No. 2014CB238902), and the “111” Project (No. B17042). This work is also in part supported by Liu Baojun Geological Science Foundation for Young Scholars (No. DMSM2017079). Special thanks are given to Xiaolin Song from Yunnan Institute of Coal Geology Prospection (China) and Peipei Wang and Hongjian Song from China University of Mining and Technology (Beijing) for their great help with sample collection. We are grateful to Shifeng Dai and Baruch Spiro for their valuable comments and suggestions during the manuscript preparation. We are indebted to two anonymous reviewers for their useful suggestions, which greatly improved the quality of the paper.

**Author Contributions:** Xue Zheng and Jingjing Liu conceived and designed the experiments; Zhen Wang, Yaguang Xu, Lei Wang and Xue Zheng performed the experiments; Xue Zheng and Jingjing Liu analyzed the data; Xue Zheng wrote the paper.

**Conflicts of Interest:** The authors declare no conflict of interest.

## References

1. Dai, S.; Zeng, R.; Sun, Y. Enrichment of arsenic, antimony, mercury, and thallium in a late Permian anthracite from Xingren, Guizhou, southwest China. *Int. J. Coal Geol.* **2006**, *66*, 217–226. [[CrossRef](#)]
2. Dai, S.; Ren, D.; Chou, C.-L.; Li, S.; Jiang, Y. Mineralogy and geochemistry of the No. 6 coal (Pennsylvanian) in the Junger Coalfield, Ordos Basin, China. *Int. J. Coal Geol.* **2006**, *66*, 253–270. [[CrossRef](#)]
3. Hower, J.C.; Ruppert, L.F.; Eble, C.F. Lanthanide, yttrium, and zirconium anomalies in the fire clay coal bed, eastern Kentucky. *Int. J. Coal Geol.* **1999**, *39*, 141–153. [[CrossRef](#)]
4. Zhao, L.; Ward, C.R.; French, D.; Graham, I.T. Mineralogical composition of late Permian coal seams in the Songzao Coalfield, southwestern China. *Int. J. Coal Geol.* **2013**, *116*, 208–226. [[CrossRef](#)]
5. Yudovich, Y.E.; Ketris, M.P. Arsenic in coal: A review. *Int. J. Coal Geol.* **2005**, *61*, 141–196. [[CrossRef](#)]
6. Karayığit, A.I.; Spears, D.A.; Booth, C.A. Antimony and arsenic anomalies in the coal seams from the Gokler coalfield, Gediz, Turkey. *Int. J. Coal Geol.* **2000**, *44*, 1–17. [[CrossRef](#)]
7. Karayığit, A.I.; Bircan, C.; Mastalerz, M.; Oskay, R.G.; Querol, X.; Lieberman, N.R.; Türkmen, İ. Coal characteristics, elemental composition and modes of occurrence of some elements in the İsaalan coal (Balıkesir, NW Turkey). *Int. J. Coal Geol.* **2017**, *172*, 43–59. [[CrossRef](#)]
8. Ren, D.; Zhao, F.; Wang, Y.; Yang, S. Distributions of minor and trace elements in Chinese coals. *Int. J. Coal Geol.* **1999**, *40*, 109–118. [[CrossRef](#)]
9. Ren, D.; Zhao, F.; Dai, S.; Zhang, J.; Luo, K. *Geochemistry of Trace Elements in Coal*; Science Press: Beijing, China, 2006; p. 556. (In Chinese)
10. Dai, S.; Ren, D.; Zhou, Y.; Chou, C.-L.; Wang, X.; Zhao, L.; Zhu, X. Mineralogy and geochemistry of a superhigh-organic-sulfur coal, Yanshan Coalfield, Yunnan, China: Evidence for a volcanic ash component and influence by submarine exhalation. *Chem. Geol.* **2008**, *255*, 182–194. [[CrossRef](#)]
11. Dai, S.; Ren, D.; Chou, C.-L.; Finkelman, R.B.; Seredin, V.V.; Zhou, Y. Geochemistry of trace elements in Chinese coals: A review of abundances, genetic types, impacts on human health, and industrial utilization. *Int. J. Coal Geol.* **2012**, *94*, 3–21. [[CrossRef](#)]
12. Dai, S.; Chou, C.-L.; Yue, M.; Luo, K.; Ren, D. Mineralogy and geochemistry of a late Permian coal in the Dafang Coalfield, Guizhou, China: Influence from siliceous and iron-rich calcic hydrothermal fluids. *Int. J. Coal Geol.* **2005**, *61*, 241–258. [[CrossRef](#)]
13. Dai, S.; Ren, D.; Tang, Y.; Yue, M.; Hao, L. Concentration and distribution of elements in late Permian coals from western Guizhou Province, China. *Int. J. Coal Geol.* **2005**, *61*, 119–137. [[CrossRef](#)]
14. Dai, S.; Zhou, Y.; Ren, D.; Wang, X.; Li, D.; Zhao, L. Geochemistry and mineralogy of the late Permian coals from the Songzao Coalfield, Chongqing, southwestern China. *Sci. China Ser. D Earth Sci.* **2007**, *50*, 678–688. [[CrossRef](#)]
15. Dai, S.; Wang, X.; Chen, W.; Li, D.; Chou, C.-L.; Zhou, Y.; Zhu, C.; Li, H.; Zhu, X.; Xing, Y.; et al. A high-pyrite semianthracite of late Permian age in the Songzao Coalfield, southwestern China: Mineralogical and geochemical relations with underlying mafic tuffs. *Int. J. Coal Geol.* **2010**, *83*, 430–445. [[CrossRef](#)]

16. Ren, D. Mineral matters in coal. In *Coal Petrology of China*; Han, D., Ed.; Publishing House of China University of Mining and Technology: Xuzhou, China, 1996; pp. 67–77. (In Chinese with English Abstract).
17. Wang, X. Geochemistry of late Triassic coals in the Changhe Mine, Sichuan Basin, southwestern China: Evidence for authigenic lanthanide enrichment. *Int. J. Coal Geol.* **2009**, *80*, 167–174. [[CrossRef](#)]
18. Zhang, J.; Ren, D.; Zheng, C.; Zeng, R.; Chou, C.-L.; Liu, J. Trace element abundances in major minerals of late Permian coals from southwestern Guizhou Province, China. *Int. J. Coal Geol.* **2002**, *53*, 55–64. [[CrossRef](#)]
19. Zhang, J.; Ren, D.; Zhu, Y.; Chou, C.-L.; Zeng, R.; Zheng, B. Mineral matter and potentially hazardous trace elements in coals from Qianxi fault depression area in southwestern Guizhou, China. *Int. J. Coal Geol.* **2004**, *57*, 49–61. [[CrossRef](#)]
20. Li, B.; Zhuang, X.; Li, J.; Querol, X.; Font, O.; Moreno, N. Enrichment and distribution of elements in the late permian coals from the zhina coalfield, guizhou province, southwest China. *Int. J. Coal Geol.* **2017**, *171*, 111–129. [[CrossRef](#)]
21. Dai, S.; Chekryzhov, I.Y.; Seredin, V.V.; Nechaev, V.P.; Graham, I.T.; Hower, J.C.; Ward, C.R.; Ren, D.; Wang, X. Metalliferous coal deposits in East Asia (primorye of Russia and South China): A review of geodynamic controls and styles of mineralization. *Gondwana Res.* **2016**, *29*, 60–82. [[CrossRef](#)]
22. Zhou, Y.; Ren, Y.; Bohor, B.F. Origin and distribution of tonsteins in late Permian coal seams of southwestern China. *Int. J. Coal Geol.* **1982**, *2*, 49–77. [[CrossRef](#)]
23. China Coal Geology Bureau. *Sedimentary Environments and Coal Accumulation of Late Permian Coal Formation in Western Guizhou, Southern Sichuan, and Eastern Yunnan, China*; Chongqing University Press: Chongqing, China, 1996; p. 216.
24. Zhou, Y.; Bohor, B.F.; Ren, Y. Trace element geochemistry of altered volcanic ash layers (tonsteins) in Late Permian coal-bearing formations of eastern Yunnan and western Guizhou Province, China. *Int. J. Coal Geol.* **2000**, *44*, 305–324. [[CrossRef](#)]
25. Dai, S.; Wang, X.; Zhou, Y.; Hower, J.C.; Li, D.; Chen, W.; Zhu, X. Chemical and mineralogical compositions of silicic, mafic, and alkali tonsteins in the late Permian coals from the Songzao Coalfield, Chongqing. Southwest China. *Chem. Geol.* **2011**, *282*, 29–44. [[CrossRef](#)]
26. Zhou, Y.; Ren, Y. Distribution of arsenic in coals of Yunnan Province, China, and its controlling factors. *Int. J. Coal Geol.* **1992**, *20*, 85–98. [[CrossRef](#)]
27. Ding, Z.; Zheng, B.; Zhang, J.; Long, J.; Belkin, H.E.; Finkelman, R.B.; Zhao, F.; Chen, C.; Zhou, D.; Zhou, Y. Geological and geochemical characteristics of high arsenic coals from endemic arsenosis areas in southwestern Guizhou Province, China. *Appl. Geochem.* **2001**, *16*, 1353–1360. [[CrossRef](#)]
28. Dai, S.; Tian, L.; Chou, C.-L.; Zhou, Y.; Zhang, M.; Zhao, L.; Wang, J.; Yang, Z.; Cao, H.; Ren, D. Mineralogical and compositional characteristics of late Permian coals from an area of high lung cancer rate in Xuanwei, Yunnan, China: Occurrence and origin of quartz and chamosite. *Int. J. Coal Geol.* **2008**, *76*, 318–327. [[CrossRef](#)]
29. Dai, S.; Chou, C.L. Occurrence and origin of minerals in a chamosite-bearing coal of late Permian age, Zhaotong, Yunnan, China. *Am. Mineral.* **2007**, *92*, 1253–1261. [[CrossRef](#)]
30. Li, Z.; Wang, D.; Lv, D.; Li, Y.; Liu, H.; Wang, P.; Liu, Y.; Liu, J.; Li, D. The geologic settings of Chinese coal deposits. *Int. Geol. Rev.* **2017**, 1–13. [[CrossRef](#)]
31. Dai, S.; Zhang, W.; Ward, C.R.; Seredin, V.V.; Hower, J.C.; Li, X.; Song, W.; Wang, X.; Kang, H.; Zheng, L.; et al. Mineralogical and geochemical anomalies of late Permian coals from the Fusui Coalfield, Guangxi Province, southern China: Influences of terrigenous materials and hydrothermal fluids. *Int. J. Coal Geol.* **2013**, *105*, 60–84. [[CrossRef](#)]
32. Dai, S.; Zhang, W.; Seredin, V.V.; Ward, C.R.; Hower, J.C.; Wang, X.; Li, X.; Song, W.; Zhao, L.; Kang, H.; et al. Factors controlling geochemical and mineralogical compositions of coals preserved within marine carbonate successions: A case study from the Heshan Coalfield, southern China. *Int. J. Coal Geol.* **2013**, *109*, 77–100. [[CrossRef](#)]
33. Dai, S.; Ren, D.; Ma, S. The cause of endemic fluorosis in western Guizhou Province, Southwest China. *Fuel* **2004**, *83*, 2095–2098. [[CrossRef](#)]
34. Dai, S.; Ren, D. Fluorine concentration of coals in China—An estimation considering coal reserves. *Fuel* **2006**, *85*, 929–935. [[CrossRef](#)]
35. Dai, S.; Finkelman, R.B. Coal as a promising source of critical elements: Progress and future prospects. *Int. J. Coal Geol.* **2017**, in press. [[CrossRef](#)]

36. Dai, S.; Yan, X.; Ward, C.R.; Hower, J.C.; Zhao, L.; Wang, X.; Zhao, L.; Ren, D.; Finkelman, R.B. Valuable elements in Chinese coals: A review. *Int. Geol. Rev.* **2016**. [[CrossRef](#)]
37. Zhao, L.; Dai, S.; Graham, I.T.; Li, X.; Zhang, B. New insights into the lowest Xuanwei Formation in eastern Yunnan Province, SW China: Implications for emeishan large igneous province felsic tuff deposition and the cause of the end-guadalupian mass extinction. *Lithos* **2016**, *264*, 375–391. [[CrossRef](#)]
38. Zhao, L.; Dai, S.; Graham, I.T.; Wang, P. Clay mineralogy of coal-hosted Nb-Zr-REE-Ga mineralized beds from Late Permian strata, eastern Yunnan, SW China: Implications for paleotemperature and origin of the micro-quartz. *Minerals* **2016**, *6*, 45. [[CrossRef](#)]
39. Zhao, L.; Dai, S.; Graham, I.T.; Li, X.; Liu, H.; Song, X.; Hower, J.C.; Zhou, Y. Cryptic sediment-hosted critical element mineralization from eastern Yunnan Province, southwestern China: Mineralogy, geochemistry, relationship to emeishan alkaline magmatism and possible origin. *Ore Geol. Rev.* **2017**, *80*, 116–140. [[CrossRef](#)]
40. Zou, J.; Tian, H.; Wang, Z. Leaching process of Rare Earth Elements, gallium and niobium in a coal-bearing strata-hosted rare metal deposit—A case study from the Late Permian tuff in the Zhongliangshan Mine, Chongqing. *Metals* **2017**, *7*, 174. [[CrossRef](#)]
41. Ali, J.R.; Fitton, J.G.; Herzberg, C. Emeishan large igneous province (SW China) and the mantle-plume up-doming hypothesis. *J. Geol. Soc.* **2010**, *167*, 953–959. [[CrossRef](#)]
42. He, B.; Xu, Y.; Chung, S.; Xiao, L.; Wang, Y. Sedimentary evidence for a rapid, kilometer-scale crustal doming prior to the eruption of the Emeishan flood basalts. *Earth Planet. Sci. Lett.* **2003**, *213*, 391–405. [[CrossRef](#)]
43. Shellnutt, J.G. The Emeishan large igneous province: A synthesis. *Geosci. Front.* **2014**, *5*, 369–394. [[CrossRef](#)]
44. Xu, Y.; Chung, S.-L.; Jahn, B.-M.; Wu, G. Petrologic and geochemical constraints on the petrogenesis of Permian Triassic Emeishan flood basalts in southwestern China. *Lithos* **2001**, *58*, 145–168. [[CrossRef](#)]
45. He, B.; Xu, Y.; Huang, X.; Luo, Z.; Shi, Y.; Yang, Q.; Yu, S. Age and duration of the Emeishan flood volcanism, SW China: Geochemistry and SHRIMP zircon U–Pb dating of silicic ignimbrites, post-volcanic Xuanwei Formation and clay tuff at the Chaotian section. *Earth Planet. Sci. Lett.* **2007**, *255*, 306–323. [[CrossRef](#)]
46. Wignall, P.B. Large igneous provinces and mass extinctions. *Earth-Sci. Rev.* **2001**, *53*, 1–33. [[CrossRef](#)]
47. Dai, S.; Seredin, V.V.; Ward, C.R.; Hower, J.C.; Xing, Y.; Zhang, W.; Song, W.; Wang, P. Enrichment of U–Se–Mo–Re–V in coals preserved within marine carbonate successions: Geochemical and mineralogical data from the late Permian Guiding Coalfield, Guizhou, China. *Miner. Deposita* **2014**, *50*, 159–186. [[CrossRef](#)]
48. Dai, S.; Li, T.; Seredin, V.; Ward, C.R.; Hower, J.C.; Zhou, Y.; Zhang, M.; Song, X.; Song, W.; Zhao, C. Origin of minerals and elements in the Late Permian coals, tonsteins, and host rocks of the Xinde Mine, Xuanwei, eastern Yunnan, China. *Int. J. Coal Geol.* **2014**, *121*, 53–78. [[CrossRef](#)]
49. Dai, S.; Xie, P.; Jia, S.; Ward, C.R.; Hower, J.C.; Yan, X.; French, D. Enrichment of U–Re–V–Cr–Se and rare earth elements in the late Permian coals of the Moxinpo Coalfield, Chongqing, China: Genetic implications from geochemical and mineralogical data. *Ore Geol. Rev.* **2017**, *80*, 1–17. [[CrossRef](#)]
50. Mahoney, J.J.; Coffin, M.F. *Large Igneous Provinces: Continental, Oceanic, and Planetary Flood Volcanism*; American Geophysical Union: Washington, DC, USA, 1997; ISBN 0-87590-082-8.
51. Courtillot, V.; Jaupart, C.; Manighetti, I.; Tapponnier, P.; Besse, J. On causal links between flood basalts and continental breakup. *Earth Planet. Sci. Lett.* **1999**, *166*, 177–195. [[CrossRef](#)]
52. Xu, Y. Evidence for crustal components in the mantle and constraints on crustal recycling mechanisms pyroxenite xenoliths from Hannuoba North China. *Chem. Geol.* **2002**, *182*, 301–322. [[CrossRef](#)]
53. Chung, S.-L.; Jahn, B.-M. Plume-lithosphere interaction in generation of the Emeishan flood basalts at the Permian-Triassic boundary. *Geology* **1995**, *23*, 889–892. [[CrossRef](#)]
54. Chung, S.L.; Jahn, B.M.; Genyao, W.; Lo, C.H.; Bolin, C. The Emeishan flood basalt in sw China: A mantle plume initiation model and its connection with continental breakup and mass extinction at the Permian-Triassic boundary. *Geodynamics* **1998**, 47–58. [[CrossRef](#)]
55. ASTM International. *Test Method for Moisture in the Analysis Sample of Coal and Coke*; ASTM D3173-11; ASTM International: West Conshohocken, PA, USA, 2011.
56. ASTM International. *Test Method for Volatile Matter in the Analysis Sample of Coal and Coke*; ASTM D3175-11; ASTM International: West Conshohocken, PA, USA, 2011.
57. ASTM International. *Test Method for Ash in the Analysis Sample of Coal and Coke from Coal*; ASTM D3174-11; ASTM International: West Conshohocken, PA, USA, 2011.
58. ASTM International. *Test Methods for Total Sulfur in the Analysis Sample of Coal and Coke*; ASTM D3177-02; ASTM International: West Conshohocken, PA, USA, 2011.

59. ASTM International. *Test Methods for Forms of Sulfur in the Analysis Sample of Coal and Coke*; ASTM D2492-02; ASTM International: West Conshohocken, PA, USA, 2007.
60. ASTM International. *Standard Test Method for Microscopical Determination of the Vitrinite Reflectance of Coal*; ASTM Standard D2798-11a; ASTM International: West Conshohocken, PA, USA, 2011.
61. Li, X.; Dai, S.; Zhang, W.; Li, T.; Zheng, X.; Chen, W. Determination of As and Se in coal and coal combustion products using closed vessel microwave digestion and collision/reaction cell technology (CCT) of inductively coupled plasma mass spectrometry (ICP-MS). *Int. J. Coal Geol.* **2014**, *124*, 1–4. [[CrossRef](#)]
62. ASTM International. *Standard Practice for Total Fluorine in Coal and Coke by Pyrohydrolytic Extraction and Ion Selective Electrode or Ion Chromatograph Methods*; ASTM Standard D5987-96; ASTM International: West Conshohocken, PA, USA, 2007.
63. Coal Analysis Laboratory of China Coal Research Institute. *Chinese Standard Method GB/T 15224.1-2010, Classification for Quality of Coal. Part 1: Ash*; Standardization Administration of China: Beijing, China, 2010. (In Chinese)
64. Chou, C.-L. Sulfur in coals: A review of geochemistry and origins. *Int. J. Coal Geol.* **2012**, *100*, 1–13. [[CrossRef](#)]
65. ASTM International. *Standard Classification of Coals by Rank*; ASTM D388-12; ASTM International: West Conshohocken, PA, USA, 2012.
66. Ketris, M.P.; Yudovich, Y.E. Estimations of clarkes for carbonaceous biolithes: World averages for trace element contents in black shales and coals. *Int. J. Coal Geol.* **2009**, *78*, 135–148. [[CrossRef](#)]
67. Grigoriev, N. *Chemical Element Distribution in the Upper Continental Crust*; UB RAS: Ekaterinburg, Russia, 2009; Volume 382, p. 383.
68. Seredin, V.V.; Dai, S. Coal deposits as potential alternative sources for lanthanides and yttrium. *Int. J. Coal Geol.* **2012**, *94*, 67–93. [[CrossRef](#)]
69. Taylor, S.R.; McLennan, S.M. *The Continental Crust: Its Composition and Evolution*; Blackwell: Oxford, UK, 1985; p. 312.
70. Dai, S.; Graham, I.T.; Ward, C.R. A review of anomalous rare earth elements and yttrium in coal. *Int. J. Coal Geol.* **2016**, *159*, 82–95. [[CrossRef](#)]
71. Xiao, L.; Xu, Y.; Mei, H.; Zheng, Y.; He, B.; Pirajno, F. Distinct mantle sources of low-Ti and high-Ti basalts from the western Emeishan large igneous province, SW China: Implications for plume–lithosphere interaction. *Earth Planet. Sci. Lett.* **2004**, *228*, 525–546. [[CrossRef](#)]
72. Ward, C.R.; Spears, D.; Booth, C.A.; Staton, I.; Gurba, L.W. Mineral matter and trace elements in coals of the Gunnedah Basin, New South Wales, Australia. *Int. J. Coal Geol.* **1999**, *40*, 281–308. [[CrossRef](#)]
73. Dai, S.; Wang, X.; Seredin, V.V.; Hower, J.C.; Ward, C.R.; O’Keefe, J.M.K.; Huang, W.; Li, T.; Li, X.; Liu, H.; et al. Petrology, mineralogy, and geochemistry of the ge-rich coal from the Wulantuga ge ore deposit, Inner Mongolia, China: New data and genetic implications. *Int. J. Coal Geol.* **2012**, *90–91*, 72–99. [[CrossRef](#)]
74. Dai, S.; Wang, P.; Ward, C.R.; Tang, Y.; Song, X.; Jiang, J.; Hower, J.C.; Li, T.; Seredin, V.V.; Wagner, N.J.; et al. Elemental and mineralogical anomalies in the coal-hosted ge ore deposit of Lincang, Yunnan, southwestern China: Key role of N<sub>2</sub>–CO<sub>2</sub>-mixed hydrothermal solutions. *Int. J. Coal Geol.* **2015**, *152*, 19–46. [[CrossRef](#)]
75. Kortenski, J.; Kostova, I. Occurrence and morphology of pyrite in Bulgarian coals. *Int. J. Coal Geol.* **1996**, *29*, 273–290. [[CrossRef](#)]
76. Karayığit, A.I.; Littke, R.; Querol, X.; Jones, T.; Oskay, R.G.; Christanis, K. The Miocene coal seams in the Soma Basin (W. Turkey): Insights from coal petrography, mineralogy and geochemistry. *Int. J. Coal Geol.* **2017**, *173*, 110–128. [[CrossRef](#)]
77. Querol, X.; Chinenon, S.; Lopez-Soler, A. Iron sulphide precipitation sequence in Albian coals from the Maestrazgo basin, southeastern Iberian range, northeastern Spain. *Int. J. Coal Geol.* **1989**, *11*, 171–189. [[CrossRef](#)]
78. Rickard, D.; Schoonen, M.A.; Luther, G., III. Chemistry of iron sulfides in sedimentary environments. In *Geochemical Transformations of Sedimentary Sulfur*; Vairavamurthy, M.A., Schoonen, M.A.A., Eglinton, T.I., Luther, G.W., Manowitz, B., Eds.; ACS Publications: Washington DC, USA, 1995; ISBN 13: 9780841233287.
79. Luther, G.W., III. Pyrite synthesis via polysulfide compounds. *Geochim. Cosmochim. Acta* **1991**, *55*, 2839–2849. [[CrossRef](#)]
80. Dai, S.; Hower, J.C.; Ward, C.R.; Guo, W.; Song, H.; O’Keefe, J.M.K.; Xie, P.; Hood, M.M.; Yan, X. Elements and phosphorus minerals in the middle Jurassic inertinite-rich coals of the Muli Coalfield on the Tibetan Plateau. *Int. J. Coal Geol.* **2015**, *144–145*, 23–47. [[CrossRef](#)]

81. Arbuzov, S.I.; Mezhibor, A.M.; Spears, D.A.; Il'enok, S.S.; Shaldybin, M.V.; Belaya, E.V. Nature of tonsteins in the Azeisk deposit of the Irkutsk Coal Basin (Siberia, Russia). *Int. J. Coal Geol.* **2016**, *153*, 99–111. [[CrossRef](#)]
82. Spears, D.A. The origin of tonsteins, an overview, and links with seatearths, fireclays and fragmental clay rocks. *Int. J. Coal Geol.* **2012**, *94*, 22–31. [[CrossRef](#)]
83. Hayashi, K.-I.; Fujisawa, H.; Holland, H.D.; Ohmoto, H. Geochemistry of ~1.9 Ga sedimentary rocks from northeastern Labrador, Canada. *Geochim. Cosmochim. Acta* **1997**, *61*, 4115–4137. [[CrossRef](#)]
84. He, B.; Xu, Y.; Zhong, Y.; Guan, J. The Guadalupian–Lopingian boundary mudstones at Chaotian (SW China) are clastic rocks rather than acidic tuffs: Implication for a temporal coincidence between the end-Guadalupian mass extinction and the Emeishan volcanism. *Lithos* **2010**, *119*, 10–19. [[CrossRef](#)]
85. Dai, S.; Luo, Y.; Seredin, V.V.; Ward, C.R.; Hower, J.C.; Zhao, L.; Liu, S.; Zhao, C.; Tian, H.; Zou, J. Revisiting the late Permian coal from the Huayingshan, Sichuan, southwestern China: Enrichment and occurrence modes of minerals and trace elements. *Int. J. Coal Geol.* **2014**, *122*, 110–128. [[CrossRef](#)]
86. Dai, S.; Liu, J.; Ward, C.R.; Hower, J.C.; French, D.; Jia, S.; Hood, M.M.; Garrison, T.M. Mineralogical and geochemical compositions of late Permian coals and host rocks from the Guxu Coalfield, Sichuan Province, China, with emphasis on enrichment of rare metals. *Int. J. Coal Geol.* **2016**, *166*, 71–95. [[CrossRef](#)]
87. Dai, S.; Li, T.; Jiang, Y.; Ward, C.R.; Hower, J.C.; Sun, J.; Liu, J.; Song, H.; Wei, J.; Li, Q.; et al. Mineralogical and geochemical compositions of the Pennsylvanian coal in the Hailiushu Mine, Daqingshan Coalfield, Inner Mongolia, China: Implications of sediment-source region and acid hydrothermal solutions. *Int. J. Coal Geol.* **2015**, *137*, 92–110. [[CrossRef](#)]
88. Sverjensky, D.A. Europium redox equilibria in aqueous solution. *Earth Planet. Sci. Lett.* **1984**, *67*, 70–78. [[CrossRef](#)]
89. Bau, M. Rare-earth element mobility during hydrothermal and metamorphic fluid-rock interaction and the significance of the oxidation state of europium. *Chem. Geol.* **1991**, *93*, 219–230. [[CrossRef](#)]
90. Zhou, Y.; Ren, Y. Origin and geological significance of tonsteins in the late Permian coals from eastern Yunnan, China. *Yunnan Geol.* **1983**, *2*, 38–46. (In Chinese)
91. Bohor, B.F.; Triplehorn, D.M. *Tonstein: Altered volcanic ash layers in coal-bearing sequences*; Special Papers; Geological Society of America: Boulder, CO, USA, 1993; Volume 285, p. 40.
92. Burger, K.; Banelow, F.K.; Bieg, G. Pyroclastic kaolin coal-tonsteins of the Upper Carboniferous of Zonguldak and Amasra, Turkey. *Int. J. Coal Geol.* **2000**, *45*, 39–53. [[CrossRef](#)]
93. Xie, P.; Song, H.; Wei, J.; Li, Q. Mineralogical characteristics of Late Permian coals from the Yueliangtian coal mine, Guizhou, southwestern China. *Minerals* **2016**, *6*, 29. [[CrossRef](#)]
94. Liu, J.; Yang, Z.; Yan, X.; Ji, D.; Yang, Y.; Hu, L. Modes of occurrence of highly-elevated trace elements in superhigh-organic-sulfur coals. *Fuel* **2015**, *156*, 190–197. [[CrossRef](#)]
95. Zhao, L.; Zhu, Q.; Jia, S.; Zou, J.; Nechaev, V.; Dai, S. Origin of Minerals and Critical Metals in an Argillized Tuff from the Huayingshan Coalfield, Southwestern China. *Minerals* **2017**, *7*, 92. [[CrossRef](#)]
96. Ward, C.R.; Corcoran, J.F.; Saxby, J.D.; Read, H.W. Occurrence of phosphorus minerals in Australian coal seams. *Int. J. Coal Geol.* **1996**, *30*, 185–210. [[CrossRef](#)]
97. Shand, P.; Johannesson, K.H.; Chudaev, O.; Chudaeva, V.; Edmunds, W.M. Rare earth element contents of high pCO<sub>2</sub> groundwaters of Primorye, Russia: Mineral stability and complexation controls. *Water Trans.* **2005**, *51*, 161–186.
98. Zhuang, X.; Su, S.; Xiao, M.; Li, J.; Alastuey, A.; Querol, X. Mineralogy and geochemistry of the Late Permian coals in the Huayingshan coal-bearing area, Sichuan Province, China. *Int. J. Coal Geol.* **2012**, *94*, 271–282. [[CrossRef](#)]
99. Wang, X.; Dai, S.; Chou, C.L.; Zhang, M.; Wang, J.; Song, X.; Wang, W.; Jiang, Y.; Zhou, Y.; Ren, D. Mineralogy and geochemistry of Late Permian coals from the Taoshuping Mine, Yunnan Province, China: Evidences for the sources of minerals. *Int. J. Coal Geol.* **2012**, *96*, 49–59. [[CrossRef](#)]
100. Reimann, C.; De Caritat, P. *Chemical Elements in the Environment: Factsheets for the Geochemist and Environmental Scientist*, 1st ed.; Springer Science & Business Media: New York, NY, USA, 1998; p. 397, ISBN 978-3-642-72018-5.
101. Dai, S.; Hou, X.; Ren, D.; Tang, Y. Surface analysis of pyrite in the No. 9 coal seam, Wuda Coalfield, Inner Mongolia, China, using high-resolution time-of-flight secondary ion mass-spectrometry. *Int. J. Coal Geol.* **2003**, *55*, 139–150. [[CrossRef](#)]
102. Dai, S.; Ren, D.; Tang, Y.; Shao, L.; Li, S. Distribution, isotopic variation and origin of sulfur in coals in the Wuda Coalfield, Inner Mongolia, China. *Int. J. Coal Geol.* **2002**, *51*, 237–250. [[CrossRef](#)]

103. Ward, C.R. Analysis and significance of mineral matter in coal seams. *Int. J. Coal Geol.* **2002**, *50*, 135–168. [[CrossRef](#)]
104. Wang, Y.; Guo, W.; Zhang, G. Application of Some Geochemical Indicators in Determining of Sedimentary Environment of the Funing Group (Paleogene), Jin-Hu Depression, Kiangsu Province. *J. Tongji Univ.* **1979**, *2*, 51–60.
105. Elderfield, H.; Greaves, M.J. The rare earth elements in seawater. *Nature* **1982**, *296*, 214–219. [[CrossRef](#)]
106. Bau, M.; Dulski, P. Distribution of yttrium and rare-earth elements in the Penge and Kuruman iron-formations, Transvaal Supergroup, South Africa. *Precambrian Res.* **1996**, *79*, 37–55. [[CrossRef](#)]
107. Karayiğit, A.I.; Oskay, R.G.; Christanis, K.; Tunoğlu, C.; Tuncer, A.; Bulut, Y. Palaeoenvironmental reconstruction of the Çardak coal seam, SW Turkey. *Int. J. Coal Geol.* **2015**, *139*, 3–16. [[CrossRef](#)]
108. Karayiğit, A.I.; Oskay, R.G.; Tuncer, A.; Mastalerz, M.; Gümüş, B.A.; Şengüler, I.; Yaradılmış, H.; Tunolğu, C. A multidisciplinary study of the Gölbaşı–Harmanlı coal seam, SE Turkey. *Int. J. Coal Geol.* **2016**, *167*, 31–47. [[CrossRef](#)]
109. Markic, M.; Sachsenhofer, R.F. Petrographic composition and depositional environments of the Pliocene Velenje lignite seam (Slovenia). *Int. J. Coal Geol.* **1997**, *33*, 229–254. [[CrossRef](#)]
110. Oskay, R.G.; Christanis, K.; İnaner, H.; Salman, M.; Taka, M. Palaeoenvironmental reconstruction of the eastern part of the Karapınar–Ayrancı coal deposit (Central Turkey). *Int. J. Coal Geol.* **2016**, *163*, 100–111. [[CrossRef](#)]
111. Siavalas, G.; Linou, M.; Chatziapostolou, A.; Kalaitzidis, S.; Papaefthymiou, H.; Christanis, K. Palaeoenvironment of Seam I in the Marathousa Lignite Mine, Megalopolis Basin (Southern Greece). *Int. J. Coal Geol.* **2009**, *78*, 233–248. [[CrossRef](#)]
112. Ward, C.R. Minerals in bituminous coals of the Sydney Basin (Australia) and the illinois Basin (USA). *Int. J. Coal Geol.* **1989**, *13*, 455–479. [[CrossRef](#)]
113. Postma, D.J. Pyrite and siderite formation in brackish and freshwater swamp sediments. *Am. J. Sci.* **1982**, *282*, 1151–1183. [[CrossRef](#)]
114. Kortenski, J. Carbonate minerals in Bulgarian coals with different degrees of coalification. *Int. J. Coal Geol.* **1992**, *20*, 225–242. [[CrossRef](#)]



© 2017 by the authors. Licensee MDPI, Basel, Switzerland. This article is an open access article distributed under the terms and conditions of the Creative Commons Attribution (CC BY) license (<http://creativecommons.org/licenses/by/4.0/>).